Emerging Research Landscape of Altermagnetism

Libor Šmejkal,[1,2] Jairo Sinova,[1,2] and Tomas Jungwirth[2,3]

[1]*Institut für Physik, Johannes Gutenberg Universität Mainz, D-55099 Mainz, Germany*
[2]*Institute of Physics, Czech Academy of Sciences, Cukrovarnická 10, 162 00 Praha 6 Czech Republic*
[3]*School of Physics and Astronomy, University of Nottingham, Nottingham NG7 2RD, United Kingdom*

(Received 15 March 2022; revised 15 August 2022; published 8 December 2022)

Magnetism is one of the largest, most fundamental, and technologically most relevant fields of condensed-matter physics. Traditionally, two basic magnetic phases have been distinguished ferromagnetism and antiferromagnetism. The spin polarization in the electronic band structure reflecting the magnetization in ferromagnetic crystals underpins the broad range of time-reversal symmetry-breaking responses in this extensively explored and exploited type of magnets. By comparison, antiferromagnets have vanishing net magnetization. Recently, there have been observations of materials in which strong time-reversal symmetry-breaking responses and spin-polarization phenomena, typical of ferromagnets, are accompanied by antiparallel magnetic crystal order with vanishing net magnetization, typical of antiferromagnets. A classification and description based on spin-symmetry principles offers a resolution of this apparent contradiction by establishing a third distinct magnetic phase, dubbed altermagnetism. Our perspective starts with an overview of the still emerging unique phenomenology of this unconventional *d*-wave (or higher even-parity wave) magnetic phase, and of the wide array of altermagnetic material candidates. We illustrate how altermagnetism can enrich our understanding of overarching condensed-matter physics concepts and how it can have impact on prominent condensed-matter research areas.

DOI: 10.1103/PhysRevX.12.040501

Subject Areas: Condensed Matter Physics
Magnetism, Spintronics

I. INTRODUCTION

Magnetic solids are traditionally divided into two elementary phases—ferromagnets and antiferromagnets [1]. Ferromagnets, known for several millennia, are characterized by a strong macroscopic magnetization. Because of the spin polarization in the reciprocal momentum space, reflecting the magnetization order parameter in direct space, they generate a range of phenomena originating from electronic band structures with broken time-reversal ($\mathcal{T}$) symmetry and spin splitting. Antiferromagnets, on the other hand, were discovered only a century ago, because of their vanishing net magnetization, which makes them behave, in many aspects, as nonmagnetic materials. In conventional antiferromagnetism, a compensating antiparallel ordering of atomic magnetic moments in the direct physical space, i.e., the effective cancellation of atomic moments leading to the vanishingly small macroscopic net magnetization, implies the absence of any counterpart spin-polarization order parameter in the reciprocal momentum space. This makes the conventional antiferromagnets, in many aspects, akin to nonmagnetic materials and invisible to the macroscopic electrical or optical probes commonly used in ferromagnets.

Recently, diverse condensed-matter research communities have been intrigued by theoretical predictions of $\mathcal{T}$-symmetry breaking macroscopic phenomena [2–16] and spin-split band structures [2–9,13–25], which are typical of ferromagnets, in crystals with compensated antiparallel magnetic ordering, which is characteristic of antiferromagnets. The apparent ferromagnetic-antiferromagnetic dichotomy in these materials challenges the traditional division of materials by the two basic magnetic phases. A recent symmetry classification and description [16], employing a generalized symmetry formalism for describing spin arrangements on crystals [26–28], resolves this contradiction. The formalism allows for describing a broad landscape of magnetic phases by considering symmetry transformations that combine generally different operations in real and spin space. The classification based on this symmetry formalism establishes, apart from the traditional ferromagnetism and antiferromagnetism, a third distinct and comparably abundant phase [16]. This third phase is characterized by a compensated magnetic order in direct space with opposite-spin sublattices connected by crystal-rotation symmetries, and by a corresponding

Published by the American Physical Society under the terms of the Creative Commons Attribution 4.0 International license. Further distribution of this work must maintain attribution to the author(s) and the published article's title, journal citation, and DOI.

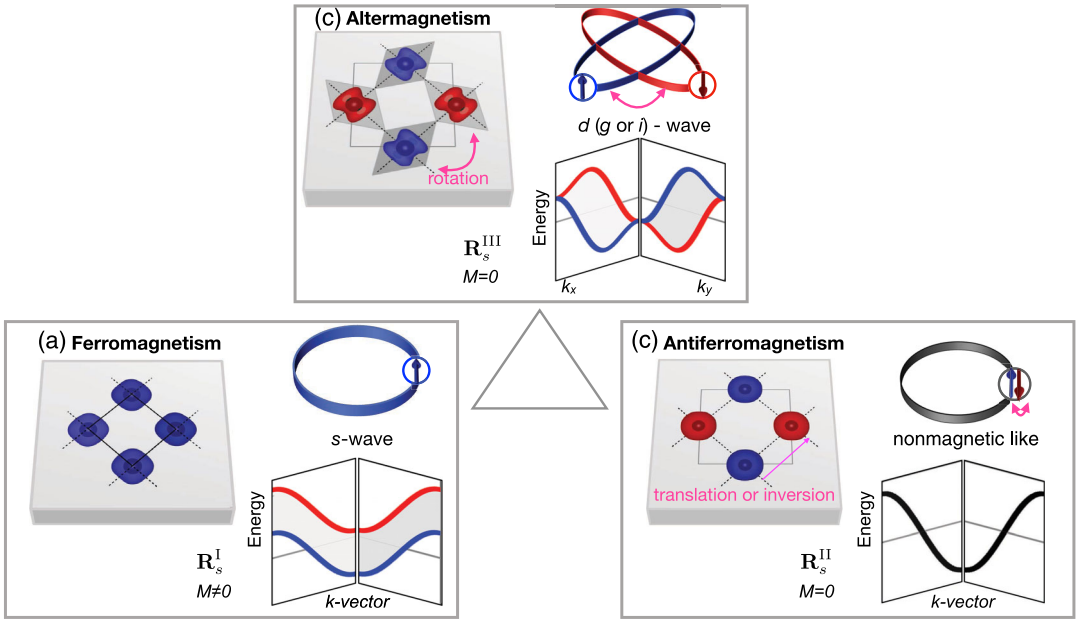

FIG. 1. Illustrative models of collinear ferromagnetism, antiferromagnetism, and altermagnetism in crystal-structure real space and nonrelativistic electronic-structure momentum space. (a) Ferromagnetic model with one spin sublattice, and corresponding distinct spin-group form, nonzero magnetization, $\mathcal{T}$-symmetry breaking momentum-independent spin splitting of bands, and isotropic s-wave spin-split Fermi surfaces. (b) Antiferromagnetic model with opposite-spin sublattices (red, blue) connected by inversion or translation, and corresponding distinct spin-group form, zero net magnetization, and $\mathcal{T}$-invariant spin-degenerate bands reminiscent of nonmagnetic systems. (c) Altermagnetic model with opposite-spin sublattices connected by rotation and not by translation or inversion, and corresponding distinct spin-group form, zero net magnetization, $\mathcal{T}$-symmetry breaking spin splitting with alternating sign, anisotropic sublattice spin densities, and anisotropic d (g or i)-wave spin-split Fermi surfaces. See Sec. II B for the definitions of the distinct spin-group forms $\mathbf{R}_s^i$.

unconventional spin-polarization order in the reciprocal momentum space that reflects the same rotation symmetries. The direct-to-reciprocal-space correspondence results in electronic band structures with broken $\mathcal{T}$ symmetry and alternating momentum-dependent sign of the spin splitting. The alternating spin polarizations in both direct physical space and reciprocal momentum space, characteristic of the third phase, suggest the term altermagnetism [16]. The distinction of the three phases is highlighted in Fig. 1.

Turning to a broader condensed-matter physics context, we point out that altermagnetism allows for a realization of unconventional d-wave magnetism, a long-sought magnetic counterpart of unconventional d-wave superconductivity [29]. Conventional superconductivity and magnetism are connected by a striking analogy [29], highlighted in Fig. 2: The electron-electron Cooper pairs forming around the Fermi surface and driving the conventional s-wave superconductivity have the counterpart in the majority spin electron—minority spin-hole pairs distributed isotropically around the Fermi surface in the conventional model of (s-wave) ferromagnetism [29]. The discovery of the unconventional d-wave superconductivity not only opened an entirely new research landscape of this many-body phase [30] but also raised a fundamental question of whether and how an unconventional d-wave counterpart could be realized in magnetism (Fig. 2) [29].

Earlier considerations focused on possible realizations of the unconventional d-wave magnetism due to strong electronic correlations [31–33]. As we will discuss, altermagnetism is a realization of the unconventional d-wave (or high even-parity wave) magnetism that emerges already on the basic level of an effective single-particle nonrelativistic description of collinear magnets. It is, therefore, a robust, elementary, magnetically ordered phase. The theoretical prediction of altermagnetism thus complements, in a fundamentally unique way, modern studies of spin quantum phases associated with more complex, and often more subtle, many-body correlations, relativistic physics, noncollinear magnetic ordering, topological phenomena, or frustrated magnetic interactions [34–43]. Simultaneously, altermagnetism can coexist and constructively interplay with these additional physical complexities.

Altermagnetism is expected to be abundant in nature and to occur in both three-dimensional and two-dimensional crystals, in diverse structural or chemistry types, and in conduction types covering the whole spectrum from insulators to superconductors. In Sec. II, we give an overview of the predicted characteristic features, symmetries, and material landscape of the altermagnetic phase.

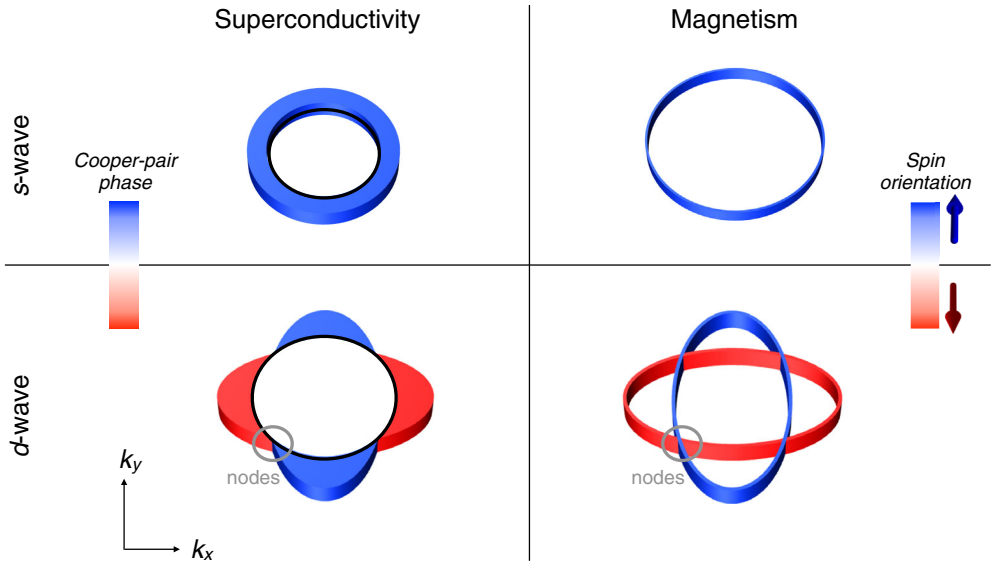

FIG. 2. Analogy between superconductivity and magnetism. Top: conventional s-wave superconductivity, which has the same Cooper-pair phase around the Fermi surface and is analogous to conventional magnetism (ferromagnetism) with an excess of one spin orientation around the Fermi surface. Bottom: unconventional d-wave superconductivity where the Cooper-pair phase changes sign around the Fermi surface, and the anticipated analogy of unconventional d-wave magnetism where the excess spin orientation changes sign around the Fermi surface. The unconventional phases have the characteristic nodes highlighted by gray circles. This figure was inspired by Ref. [29].

The properties connected to the spin-polarized $\mathcal{T}$-symmetry broken band structures of altermagnets open up a potential for previously unanticipated developments in a broad condensed-matter physics field. In Sec. III, we highlight the distinct properties of altermagnets in the context of overarching physical concepts of lifted Kramers spin degeneracy, Fermi-liquid instabilities, electron and magnon quasiparticles, and Berry phase and nondissipative transport. In Sec. IV, we outline the potential we foresee of altermagnets in selected active research areas, including spintronics, ultrafast photomagnetism, neuromorphics, thermoelectrics, field-effect electronics, multiferroics, and superconductivity.

While our focus in the following sections is on the emerging field of altermagnetism from the theory perspective, we point out here that first measurements have already indicated that altermagnetism can soon become an active experimental field. Shortly after the theoretical predictions of the possible coexistence of the compensated antiparallel magnetic order and the $\mathcal{T}$-symmetry breaking electronic responses, supporting evidence has been discovered by initial experiments [5,10–12], as highlighted in Table I. Apart from the fundamental physics interest, we expect that intense experimental research will also be driven by the potential impact of altermagnetism on technology. Altermagnetism can occur in crystals with common light elements, high-magnetic-ordering temperatures, and strong spin coherence, which are among the key prerequisites for practical device applications [16].

II. ALTERMAGNETIC PHASE

A. *Ab initio* band structures

In Fig. 3, we show representative nonrelativistic band structures of metallic RuO_2 [3,8,13,14,16,18] and insulating FeF_2 [47] and MnF_2 [20,48], on which we illustrate key characteristics of the spin-polarization order in the altermagnetic band structures that break $\mathcal{T}$ symmetry. These

TABLE I. Theoretical predictions, supported by experiments, of $\mathcal{T}$-symmetry breaking macroscopic phenomena in RuO_2, and a list of other altermagnetic materials in which these macroscopic responses were also theoretically predicted. The anomalous Hall effect is a $\mathcal{T}$-odd off-diagonal component of the electrical conductivity tensor [2]. The $\mathcal{T}$-odd spin current can be generated along or transverse to an applied electrical bias; an out-of-plane spin current generated by an in-plane electrical bias in an altermagnetic layer can exert a torque on magnetic moments in an adjacent layer in a multilayer stack [8].

Macroscopic response	Theory in RuO_2	Experiment in RuO_2	Theory in other materials
Anomalous Hall effect	2019 [3]	2020 [5]	$SrRuO_3$ [44], Mn_5Si_3 [6], κ-Cl [45], (Cr,Fe)Sb_2 [7], perovskites [46]
Spin current and torque	2020 [8,16]	2021 [10–12]	κ-Cl [4], $CaCrO_3$ [9]

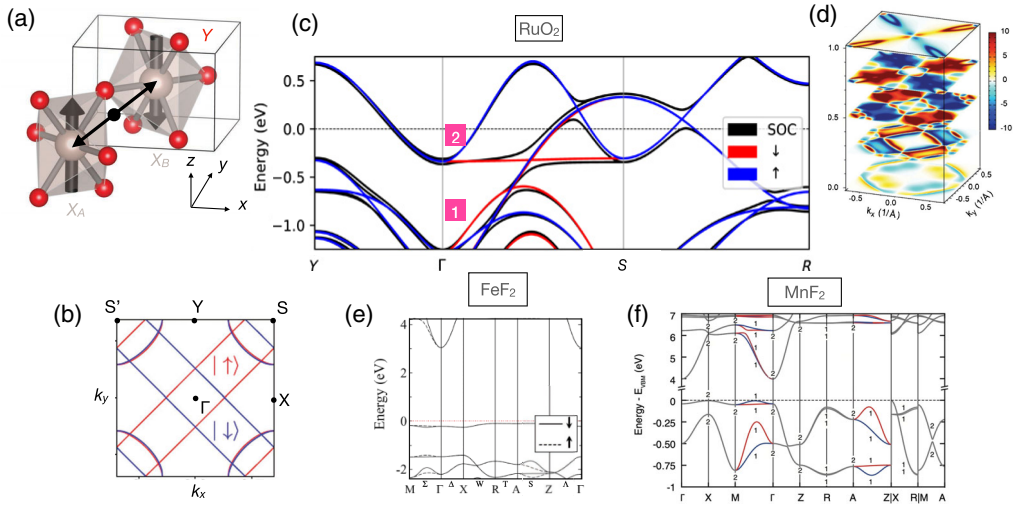

FIG. 3. (a) Schematics of the rutile XY_2 crystal structure with antiparallel magnetic moments on X_A and X_B magnetic sublattices. (b) Brillouin zone of the rutile crystal and *ab initio* nonrelativistic calculation of a wave-vector $k_z = 0$ cut of the anisotropic *d*-wave spin-polarized Fermi surface of metallic RuO_2. (c) *Ab initio* altermagnetic spin splitting of bands in RuO_2, calculated without (red and blue) and with (black) relativistic spin-orbit coupling. (d) *Ab initio* altermagnetic spin-split Fermi surface for selected k_z values in RuO_2 with correlations accounted for within the dynamical mean-field theory. (d,e) *Ab initio* altermagnetic spin-split bands of insulating FeF_2 and MnF_2, respectively. This figure is adapted from Refs. [3,18,20,47].

altermagnetic material examples belong to the family of crystals with rutile structure [Fig. 3(a)]. For several insulating members of the rutile family, the compensated antiparallel arrangement of magnetic moments [Fig. 3(a)] was well known already to Néel and his contemporaries who, ironically, introduced them into the literature as a classic representation of antiferromagnetism [49,50]. The notion was based on focusing on the lattice of magnetic atoms alone while omitting the essential role of nonmagnetic atoms on magnetism in the rutile crystals. This may be one of the reasons why the unconventional spin-polarization order in the reciprocal momentum space, resulting in the $\mathcal{T}$-symmetry breaking and alternating spin splitting of their nonrelativistic band structures [Figs. 3(b)–3(f)], remained unnoticed for nearly a century.

Remarkably, the room-temperature antiparallel magnetic ordering in metallic rutile RuO_2 was discovered [51,52] and investigated [53,54] only recently. The subsequent theoretical and experimental exploration of the $\mathcal{T}$-symmetry breaking electronic responses [3,5,8,10–14,16,18,19] has made RuO_2 one of the workhorse materials of the emerging research of altermagnetism.

Figures 3(b)–3(f) show that the altermagnetic spin splitting is strongly momentum dependent in all three rutiles. In RuO_2, it reaches, in parts of the Brillouin zone, close to 1-eV scale, which is comparable to the spin-splitting magnitudes in ferromagnets. Unlike ferromagnets, however, the altermagnetic spin splitting in the nonrelativistic bands is accompanied by a symmetry-protected zero net magnetization.

Figure 3 also illustrates that spin splittings in altermagnets, which are of the strong nonrelativistic origin, can exceed, by an order of magnitude, the record relativistic spin splittings in bulk crystals with heavy elements [55]. Moreover, unlike the momentum-dependent spin textures in the relativistic bands, spin is a good quantum number, and the electronic states share a common momentum-independent spin quantization axis in the nonrelativistic bands of altermagnets.

The spin-split parts of the altermagnetic band structure are accompanied by spin degeneracies along certain surfaces in the Brillouin zone. In Sec. II B, we show that the altermagnetic spin-group symmetries of the given crystal characterize the prominent symmetries of the spin-polarization order in the electronic band structure [16].

Fermi-surface cuts shown in Figs. 3(b) and 3(d) highlight the typical anisotropic nature of the spin-polarized Fermi surfaces, with an equal number of states in the opposite spin channels, and with spin-momentum locking that is even under the inversion of the momentum and breaks $\mathcal{T}$ symmetry.

The altermagnetic phase is robust in a broad range of materials, as it can be described within the effective single-particle Kohn-Sham theory, and the nonrelativistic crystal potential can play a dominant role in both uncorrelated and correlated, and in both clean and disordered altermagnets. This is illustrated, for example, by *ab initio* calculations in RuO_2 shown in Figs. 3(c) and 3(d). The calculations demonstrate that the altermagnetic spin splitting is only weakly affected by the relativistic spin-orbit coupling and that the prominent features of the altermagnetic spin-momentum locking are preserved when including correlation effects beyond the local-spin-density approximation of the density-functional theory [3,18,20]. A stable itinerant

altermagnetism is further confirmed in calculations without Hubbard correlations in other material candidates, such as Mn_5Si_3 [6] or KRu_4O_8 [16]. A sizable altermagnetic spin splitting also survives in the presence of a strong alloying disorder, as shown in altermagnetic $Cr_{0.15}Fe_{0.85}Sb_2$ [7]. This robustness can be understood by the fact that the altermagnetic spin-group symmetries, discussed in the following section, can hold equally well for the effective single-particle Kohn-Sham potential, as well as for the Dyson-equation description of many-body systems.

B. Symmetry classification and description

We now move from the microscopic *ab initio* theory to a symmetry-based framework for classification and description of altermagnetism as a distinct phase from ferromagnetism and antiferromagnetism [16]. The framework allows for describing a broad landscape of phases by considering symmetry transformations in real space, or in spin space, or transformations that combine generally different operations in real and spin space [26–28]. Classical examples of the first two cases are liquid and solid phases of matter, distinguished by the presence vs absence of a real-space rotation symmetry, and nonmagnetic vs ferromagnetic phases, distinguished by the presence vs absence of a spin-space rotation symmetry. Below, we show that the classification and description of the distinct ferromagnetic, antiferromagnetic, and altermagnetic phases will consider the combinations of generally different operations acting simultaneously in real and spin space [16].

Microscopically, the above symmetry formalism corresponds to nonrelativistic quantum mechanics in which real space and spin space are decoupled. In magnetism, nonrelativistic physics typically dominates over the relativistic spin-orbit coupling [26,56]. Nevertheless, the corresponding nonrelativistic spin-group formalism [26–28] has been employed only sporadically in the magnetic literature [16,24,25,56–61], in contrast to the commonly employed relativistic magnetic groups [62–67].

The nonrelativistic spin groups consider pairs of transformations $[R_i\|R_j]$, where the transformation on the left of the double vertical bar acts only in spin space, and the generally different transformation on the right of the double vertical bar simultaneously acts only in real space; an example is the important spin-group symmetry of RuO_2, $[C_2\|C_{4z}\boldsymbol{t}]$, highlighted in Fig. 4(a), which combines a twofold spin-space rotation with a fourfold real-space rotation (nonsymmorphic with translation labeled by $\boldsymbol{t}$). In contrast, the relativistic magnetic groups contain only the same transformations acting simultaneously in spin and real space, $R_i \equiv [R_i\|R_i]$ [26–28]. Therefore, the magnetic groups cover a much narrower symmetry landscape than the spin groups. Correspondingly, the relativistic magnetic groups can omit phases and phenomena that emerge when considering the richer nonrelativistic spin-group formalism. For example, the magnetic groups principally omit the

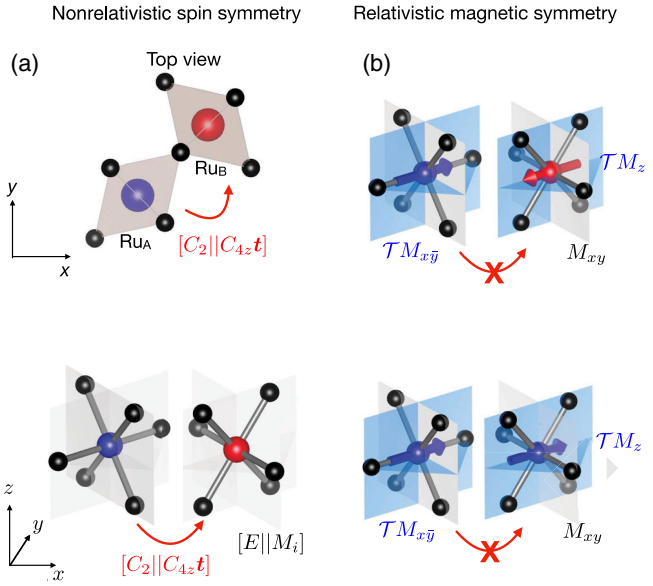

FIG. 4. (a) Schematic top view (upper panel) and 3D view (lower panel) of the RuO_2 crystal with opposite spin directions on Ru_A and Ru_B sublattices depicted in red and blue, oxygen atoms shown in black, and with the depicted nonrelativistic spin-group symmetries corresponding to spin group ${}^{2}4/{}^{1}m{}^{2}m{}^{1}m$ in the notation of Ref. [16]. The curved red arrow and its label highlight the generator of opposite-spin sublattice transformations, and the generators of the halving subgroup of same-spin sublattice transformations are also highlighted (in black). Here, C_2 on the left of the double vertical bar is a 180° spin-space rotation transformation around an axis perpendicular to the spins, and E is the spin-space identity. On the right of the double vertical bar, $C_{4z}\boldsymbol{t}$ is a fourfold real-space rotation combined with translation, and M_i are real-space mirror transformations. (b) Schematic spin arrangement on the RuO_2 crystal with antiparallel (upper panel) and parallel (lower panel) spin directions and the crystallographic spin-axis orientation depicted by red and blue arrows, and with the depicted generators of the relativistic magnetic symmetry group $m'm'm$. Here, $\mathcal{T}$ is time reversal. The crossed arrow highlights that the magnetic group contains no opposite spin-sublattice transformation elements. The same magnetic group describes a fully compensated antiparallel magnetic order, a parallel magnetic order with a strong nonrelativistic ferromagnetic moment, as well as an antiparallel magnetic order with a weak uncompensated relativistic magnetization [16]. This example illustrates that the relativistic magnetic groups generally do not separate between relativistic and nonrelativistic, compensated and noncompensated, or collinear and noncollinear magnetic phases. This figure is adapted from Ref. [16].

$[C_2\|C_{4z}\boldsymbol{t}]$ spin symmetry [Fig. 4(b)]. This symmetry, however, signals the unconventional d-wave magnetic phase in RuO_2 and governs prominent responses, such as the giant magnetoresistance [13,16].

A recent theoretical development has shown that the spin groups lead to the classification and description of three distinct phases of collinear magnetism [16] (Fig. 1): The first phase has one spin lattice (or opposite-spin sublattices

TABLE II. Spin-group symmetries and corresponding magnetic crystal-structure and nonrelativistic band-structure characteristics. The first two lines regard symmetries that apply to all three nonrelativistic collinear phases. The remaining lines apply only to altermagnets. For the definitions of symbols in the first column, see Sec. II B. This table is adapted from Ref. [16].

Spin-group symmetries	Magnetic crystal structure	Nonrelativistic band structure
$[\mathbf{C}_\infty\|E]$	Collinear	Spin is a good quantum number and $\mathbf{k}$ independent
$[\bar{C}_2\|\mathcal{T}]$	Coplanar	Invariance under inversion of $\mathbf{k}$
$[E\|\mathbf{H}]$	Sublattice spin-density anisotropy	Spin-Fermi-surface anisotropy
$[C_2\|A\mathbf{H}]$	Compensated	Broken $\mathcal{T}$ and spin splitting at general $\mathbf{k}$
$\mathbf{L}_\mathbf{k} \cap A\mathbf{H} \neq \varnothing$		Spin degeneracy at high-symmetry $\mathbf{k}$
$\mathbf{L}_\mathbf{k} \cap A\mathbf{H} = \varnothing$		$+/-$ spin splitting at general $\mathbf{k}/A\mathbf{H}\mathbf{k}$

not connected by any symmetry transformation). It corresponds to conventional ferromagnetism (ferrimagnetism) [62]. The second phase has opposite-spin sublattices connected by translation or inversion and corresponds to conventional antiferromagnetism [1,26,68]. The third phase has opposite-spin sublattices connected by rotation (proper or improper and symmorphic or nonsymmorphic) but not connected by translation or inversion.

The conventional ferromagnetic phase has a net magnetization of a strong nonrelativistic origin in the direct physical space and a corresponding spin-polarization order in the reciprocal momentum space that is principally isotropic (s wave) [Fig. 1(a)]. The electronic structure is split into majority-spin and minority-spin bands that break $\mathcal{T}$ symmetry [62]. The conventional antiferromagnetic phase has a staggered order of the magnetic moments in the direct space of a strong nonrelativistic origin with a zero net magnetization and no corresponding spin-polarization order in the reciprocal momentum space [Fig. 1(b)]. The electronic energy bands are spin degenerate and $\mathcal{T}$ invariant in the limit of zero relativistic spin-orbit coupling, reminiscent of nonmagnetic systems [1,69–73]. The third, altermagnetic phase has an alternating order of the magnetic moments in the direct space of a strong nonrelativistic origin with a zero net magnetization in the limit of zero relativistic spin-orbit coupling, and a corresponding alternating spin-polarization order in the reciprocal momentum space [Fig. 1(c)]. The spin-up and spin-down energy bands are split, break $\mathcal{T}$ symmetry, and are equally populated in the limit of zero relativistic spin-orbit coupling [16].

The spin groups contain both symmetries that are common to all three collinear magnetic phases (so-called spin-only groups) and symmetries corresponding exclusively to one of the three phases (so-called nontrivial spin groups) [16]. Among the common symmetries, arbitrary rotations of the spin space around the axis of spins ($[\mathbf{C}_\infty\|E]$ with E on the right of the double vertical bar denoting the real-space identity transformation) [16,27] protect spin as a good quantum number with a momentum-independent spin-quantization axis across the whole Brillouin zone. The energy bands $\epsilon(s,\mathbf{k})$ can then be indexed by the spin s, and the electronic structure is strictly separated into nonmixing spin-up and spin-down channels [16], as highlighted on the first line of Table II. Since all collinear magnetic orderings are coplanar, they also have the coplanarity symmetry ($[\bar{C}_2\|\mathcal{T}]$) combining the spin-space inversion, i.e., time reversal, with the 180° spin-space rotation around an axis perpendicular to the spins [16,27]. This symmetry protects a general invariance of the nonrelativistic electronic energy bands under real-space (crystal-momentum) inversion, i.e., $\epsilon(s,\mathbf{k}) = \epsilon(s,-\mathbf{k})$ [16] (second line of Table II).

The nontrivial spin groups that are specific exclusively to the nonrelativistic electronic energy bands of altermagnets are given by Ref. [16], $\mathbf{R}_s^{\mathrm{III}} = [E\|\mathbf{H}] + [C_2\|\mathbf{G}-\mathbf{H}] = [E\|\mathbf{H}] + [C_2\|A\mathbf{H}]$. Here, E on the left of the double vertical bar denotes the spin-space identity transformation, and $\mathbf{H}$ is a subgroup containing half of the real-space transformations of the nonmagnetic crystallographic group $\mathbf{G}$ (including the real-space identity). The remaining half of the transformations, $\mathbf{G}-\mathbf{H}$, can be written as $A\mathbf{H}$, where A is a real-space rotation (proper or improper). In contrast, the nontrivial spin groups describing the momentum-space electronic structure of the conventional ferromagnetic phase have a distinct form, $\mathbf{R}_s^{\mathrm{I}} = [E\|\mathbf{G}]$, and those of the conventional antiferromagnetic phase have another distinct form, $\mathbf{R}_s^{\mathrm{II}} = [E\|\mathbf{G}] + [C_2\|\mathbf{G}]$ [16].

Because of the inversion symmetry of bands in collinear magnets, the above classification is limited to $\mathbf{G}$'s that are crystallographic point groups (translations replaced with identity) containing the real-space inversion symmetry (crystallographic Laue groups), independent of whether the magnet does or does not have real-space inversion symmetry [16].

In altermagnets, the corresponding nontrivial spin subgroup $[E\|\mathbf{H}]$ contains symmetry transformations that interchange atoms belonging only to one of the two spin sublattices. These symmetries determine the characteristic anisotropy of the real-space sublattice spin densities and the anisotropy of the individual spin-channel Fermi surfaces (third line of Table II). Note that $\mathbf{G}-\mathbf{H} = A\mathbf{H}$ contains the other half of the real-space transformations. These are

generated by a real-space transformation A, which is, exclusively, a rotation (proper or improper) [16]. The corresponding spin-group symmetries $[C_2\|A\mathbf{H}]$ are transformations that interchange atoms between opposite-spin sublattices. The presence of symmetry transformations connecting the opposite-spin sublattices protects the zero net magnetization of the nonrelativistic magnetic structure [16] (fourth line of Table II). Simultaneously, since the symmetry transformations connecting the opposite-spin sublattices include only real-space rotations (proper or improper), they allow for broken $\mathcal{T}$ symmetry in the band structure, i.e., $\epsilon(s,\mathbf{k}) \neq \epsilon(-s,-\mathbf{k})$, and for spin splitting, i.e., $\epsilon(s,\mathbf{k}) \neq \epsilon(-s,\mathbf{k})$ [16] (fourth line of Table II).

The sign of the spin splitting alternates across the Brillouin zone, in line with the zero net magnetization, which implies the presence of spin-degenerate high-symmetry momenta in the band structure. The spin degeneracy is protected by symmetry when the little group of momentum $\mathbf{k}$ ($\mathbf{L}_\mathbf{k}$) contains at least one of the real-space symmetry transformations $A\mathbf{H}$ connecting opposite-spin sublattices [16] ($\mathbf{L}_\mathbf{k} \cap A\mathbf{H} \neq \varnothing$; see fifth line of Table II). Recall that a little group contains real-space symmetry transformations that map momentum $\mathbf{k}$ onto itself or onto a momentum that differs from $\mathbf{k}$ by a reciprocal lattice vector.

For a general momentum $\mathbf{k}$ with spin splitting allowed by symmetry ($\mathbf{L}_\mathbf{k} \cap A\mathbf{H} = \varnothing$; see sixth line of Table II), the opposite-spin equal-energy states are, at rotated momenta, given by $A\mathbf{H}\mathbf{k}$.

Reference [16] gives a list of all ten spin Laue groups $\mathbf{R}_s^{\mathrm{III}}$ (or 37 corresponding spin point groups) classifying and describing altermagnets. They are constructed from only eight different crystallographic Laue groups. The three remaining crystallographic Laue groups, $\mathbf{G} = \bar{1}$, $\bar{3}$, or $m3$, do not allow for the altermagnetic phase.

Below, we summarize the basic elements of the algorithm for determining the altermagnetic spin group, which can be constructed by identifying

(1) the crystallographic group of the material,
(2) the crystallographic group of the spin sublattice (in the case of a bipartite lattice, the spin sublattice point group corresponds directly to the Wyckoff position point group), and
(3) the crystallographic rotation transformation connecting the opposite-spin sublattices.

Taking RuO_2 as an example, the crystallographic point group $\mathbf{G} = 4/mmm$, the sublattice (Wyckoff) point group $\mathbf{H} = mmm$, and the crystallographic point-group rotation generating the symmetry transformation connecting the opposite-spin sublattices is C_{4z} [cf. Fig. 4(a)].

Finally, let us note that symmetry is one of the fundamental principles in physics for identifying distinct phases of matter [62,74] and that a phase is commonly associated with a uniform state of a physical system distinguished from other phases by, among others, crystal structure, composition, or type of order (e.g., magnetic). As a reference, we can recall how observations in the early 20th century, initially prompting conflicting notions of paramagnetic or ferromagnetic anomalies, were later resolved by Néel's symmetry-based delimitation of the antiferromagnetic phase [1]. We can compare this to the recent works that have raised conflicting notions of ferromagnetic or antiferromagnetic anomalies, and the resolution of the conflict by the symmetry-based classification and description of the third, altermagnetic phase [16].

While above we have only provided a brief summary, a detailed spin-group classification and description of altermagnetism, including a discussion within the general context of phases of condensed-matter systems, is given in Ref. [16]. Each phase in a material system exhibits a characteristic set of physical properties and responses, which, for altermagnetism, are yet to be fully explored. Our understanding of, and outlook on, the distinct phenomenology of altermagnetism in a broad context of basic and applied condensed-matter physics fields will be the focus of Secs. III and IV. First, we summarize the basic rules for identifying altermagnets and list representative material candidates.

C. Identification rules

Elementary rules for identifying the altermagnetic phase of a crystal can be summarized as follows:

(1) There is an even number of magnetic atoms in the unit cell, and the number of atoms in the unit cell does not have to change between the nonmagnetic and magnetic phases of the crystal [cf. two Ru atoms in the RuO_2 unit cell, shown in Fig. 4(a)].
(2) There is no inversion center between the sites occupied by the magnetic atoms from the opposite-spin sublattices [cf. the absence of the inversion center between the Ru_A and Ru_B sites in RuO_2 because of the oxygen atoms, shown in Fig. 4(a)].
(3) The two opposite-spin sublattices are connected by crystallographic rotation transformation, possibly combined with translation or inversion transformation [cf. the opposite-spin sublattices in RuO_2 connected by $C_{4z}\boldsymbol{t}$ transformation, shown in Fig. 4(a)].
(4) The spin group is determined by the algorithm described in Sec. II B (cf. the RuO_2 spin group with $A = C_{4z}$ and $\mathbf{H} = mmm$).

D. Material candidates

The rules from Sec. II C can be used for high-throughput scanning of altermagnetic material candidates. This section gives an overview of the predicted range of material types, illustrated on specific examples.

Symmetry prohibits the realization of altermagnetism in one-dimensional (1D) chains because of the absence

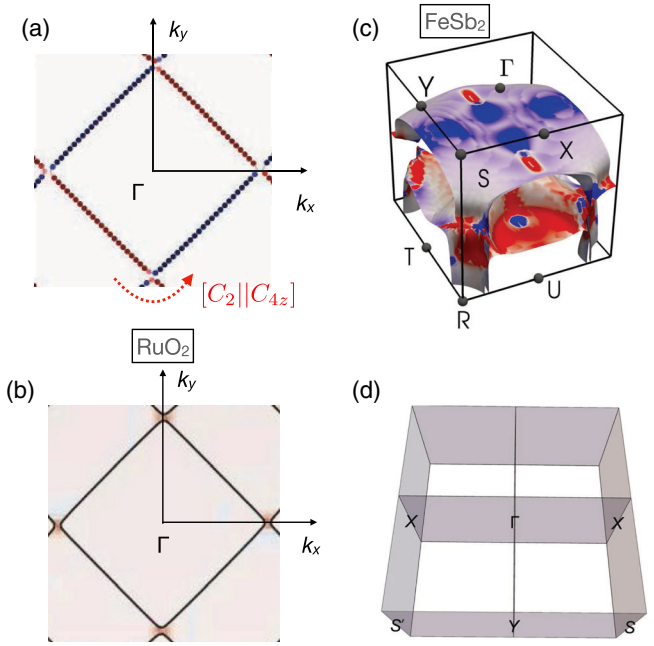

FIG. 5. (a) Spin-polarized relativistic Fermi surface highlighting the presence of the approximate spin symmetry $[C_2||C_{4z}]$, omitted by the magnetic group. (b) Relativistic momentum-resolved Berry curvature hotspots originating from the avoided crossings along the $k_{x,y} = 0$ lines, whose position in the momentum space is determined by the spin symmetries in the absence of the relativistic spin-orbit coupling. (c) Fermi-surface-resolved Berry curvature of the $FeSb_2$ altermagnet illustrates pronounced contributions to Berry curvature from the quasinodal surface $k_x = 0, k_y = 0$. (d) Brillouin zone notation. This figure is adapted from Refs. [5,7,16].

of rotation transformations in 1D. On the other hand, Figs. 6–8, and the list of material candidates given below, illustrate that altermagnetism can occur in two-dimensional (2D) and three-dimensional (3D) crystals; the conduction types can cover the whole spectrum from insulators, semiconductors, and semimetals, to metals and superconductors; and the structure and chemistry types can also be diverse:

(i) quasi-2D oxide insulator V_2Se_2O [15] or semimetal Cr_2O [75],
(ii) 3D rutile fluoride or oxide insulators FeF_2 [47], MnF_2 [20,48], MnO_2 [17], and metal RuO_2 [3,18],
(iii) perovskite oxide insulators $LaMnO_3$ [22,76], $CaCrO_3$ [9], and parent cuprate of high-T_c superconductor La_2CuO_4 [16],
(iv) ferrite insulator Fe_2O_3 [16],
(v) pnictide with metal-insulator transition $FeSb_2$ [7,16] and metal CrSb [16],
(vi) chalcogenide semiconductor MnTe [16] and (semi) metal VNb_3S_6 [16] and $CoNb_3S_6$ [3],
(vii) silicide metal Mn_5Si_3 [6],
(viii) organic insulator κ-Cl [4].

Crystallographic and spin groups, and other characteristics of the selected altermagnetic material candidates are summarized in Table III.

A list of crystallographic symmetry groups that, in principle, allow for hosting the altermagnetic phase is given in Ref. [16]. We also point out that altermagnetism can occur in structures with inversion symmetry (e.g., rutiles) or without inversion symmetry (e.g., VNb_3S_6 or $CoNb_3S_6$).

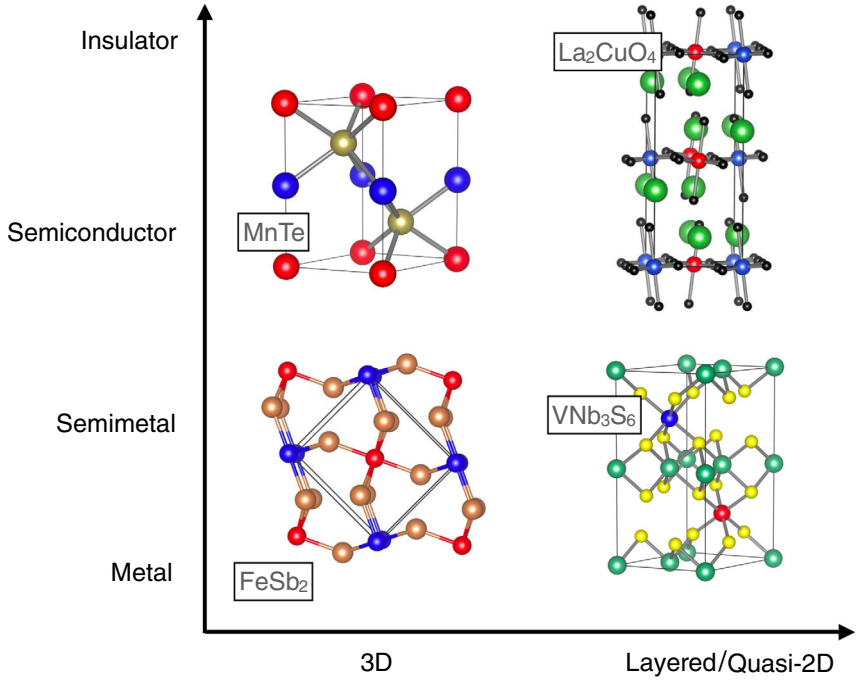

FIG. 6. Crystal structures of selected altermagnetic candidates organized by dimensionality and conduction type. The crystal structure are discussed in detail in Refs. [7,16].

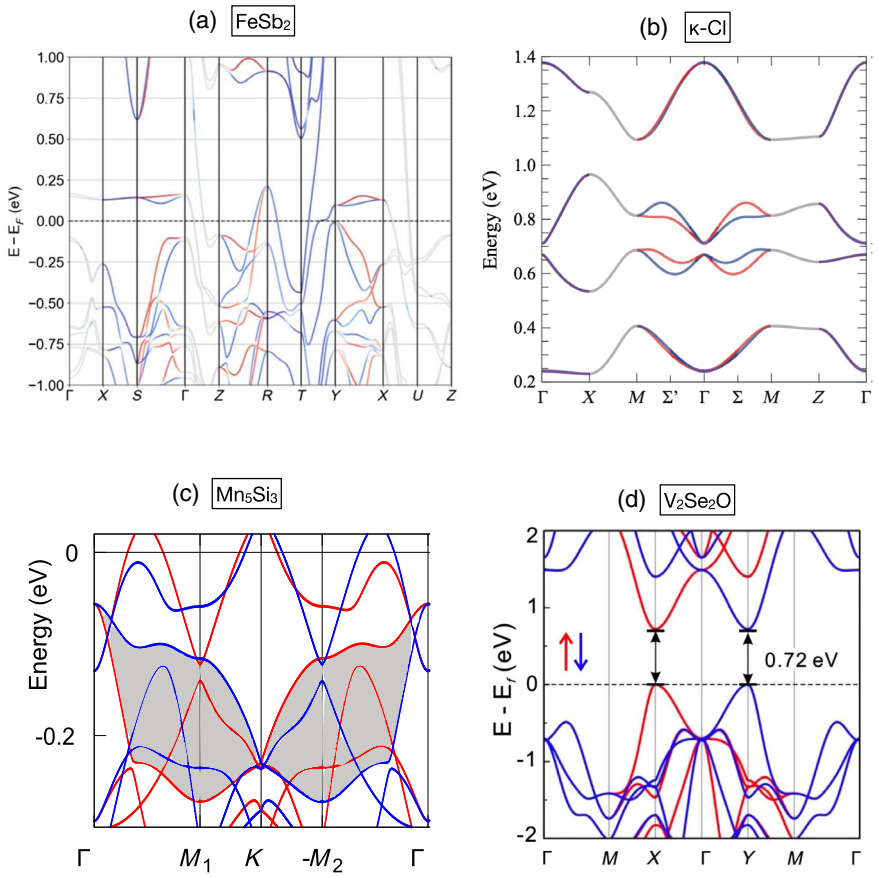

FIG. 7. (a)–(d) *Ab initio* spin-split band structures of depicted altermagnetic candidate materials. This figure is adapted from Refs. [6,7,15,116].

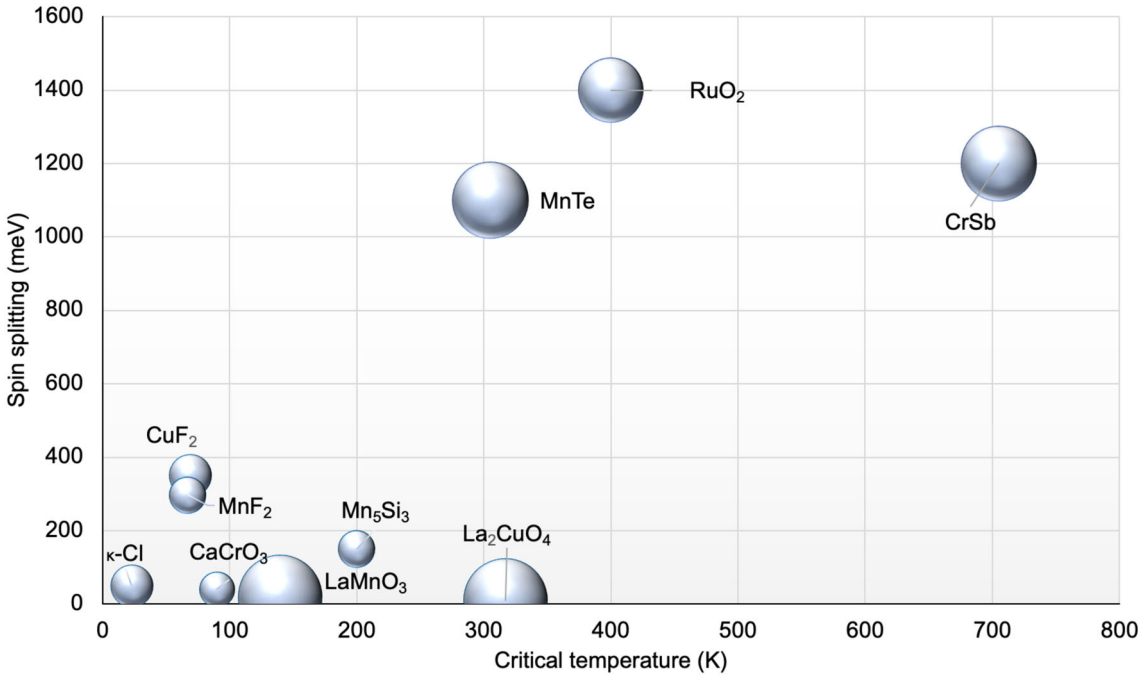

FIG. 8. Altermagnetic candidates identified from *ab initio* calculations, organized in a altermagnetic transition temperature vs altermagnetic spin-splitting strength diagram. The size of the balls scales with the largest atomic number in the crystal. This figure is adapted from Ref. [16] and references therein.

TABLE III. Altermagnetic candidates identified from *ab initio* calculations. We list the nonmagnetic space group, spin point group, even-parity wave anisotropy, metallic (M) or insulating/semiconducting (I) conduction type, altermagnetic transition temperature, and altermagnetic spin-splitting magnitude and anisotropy type.

	Space group	Spin point group	Anisotropy	Conduction	T_{AM} (K)	Splitting (meV)	References
RuO_2	$P4_2/mnm$	${}^{2}4/{}^{1}m{}^{1}m{}^{1}m$	d-wave	M	400	1400	[3,18]
KRu_4O_8	$I4/m$	${}^{2}4/{}^{1}m$	d-wave	M	⋯	300	[16]
Mn_5Si_3	$P6_3/mcm$	${}^{2}m{}^{2}m{}^{1}m$	d-wave	M	≈200	150	[6]
$(Cr,Fe)Sb_2$	$Pnma$	${}^{2}m{}^{2}m{}^{1}m$	d-wave	M	⋯	200	[7]
$CaCrO_3$	$Pnma$	${}^{2}m{}^{2}m{}^{1}m$	d-wave	M	90	200	[9]
CrSb	$P6_3/mmc$	${}^{2}6/{}^{2}m{}^{2}m{}^{1}m$	g-wave	M	705	1200	[16]
MnF_2	$P4_2/mnm$	${}^{2}4/{}^{1}m{}^{1}m{}^{1}m$	d-wave	I	67	297	[20,48]
MnO_2	$P4_2/mnm$	${}^{2}4/{}^{1}m{}^{1}m{}^{1}m$	d-wave	I	⋯	900	[17]
CuF_2	$P2_1/c$	${}^{2}2/{}^{2}m$	d-wave	I	69	350	[16]
La_2CuO_4	$Bmab$	${}^{2}m{}^{2}m{}^{1}m$	d-wave	I	317	10	[16]
$LaMnO_3$	$Pnma$	${}^{2}m{}^{2}m{}^{1}m$	d-wave	I	139,5	20	[22,76]
κ-Cl	$Pnma$	${}^{2}m{}^{2}m{}^{1}m$	d-wave	I	23	50	[4]
Fe_2O_3	$R\bar{3}c$	${}^{1}\bar{3}{}^{2}m$	g-wave	I	966	200	[16]
MnTe	$P6_3/mmc$	${}^{2}6/{}^{2}m{}^{2}m{}^{1}m$	g-wave	I	310	1100	[16]

III. PHYSICAL CONCEPTS

To illustrate the potential and stimulate future research of altermagnetism in a broad condensed-matter physics field, we now discuss our understanding of, and outlook on, unique features of the altermagnetic phase in the context of several overarching physical concepts.

A. Lifted Kramers spin degeneracy

Energy bands are Kramers spin degenerate [77,78] across the whole Brillouin zone in all crystals that are invariant under the symmetry transformation that combines $\mathcal{T}$ and space inversion. Lifting Kramers spin degeneracy by breaking the symmetry has brought forth a plethora of physically intriguing and technologically relevant phenomena, ranging from topological phases of matter [41,42,79–84] and dissipationless Hall transport [2,37,42], to charge-spin conversion effects in spintronic memory devices [40,85–87].

For the many decades of spin-physics research, lifting of the Kramers spin degeneracy in energy bands has been considered to originate from two basic mechanisms—relativistic and nonrelativistic—where the latter is due to an internal magnetization in ferromagnets or an applied magnetic field. We start by briefly recalling these two mechanisms to highlight their distinction from the unconventional mechanism in altermagnets. Before moving on to altermagnets, we also briefly review the physics of (lifted) Kramers spin degeneracy in antiferromagnets to further emphasize the distinct physics of altermagnetism.

The first conventional mechanism of lifting the Kramers spin degeneracy that does not require magnetic order links the broken space-inversion symmetry in the direct crystal space to the spin space by the electron's relativistic spin-orbit coupling [88,89]. It results in inversion-asymmetric spin-split energy bands with typically noncollinear spin textures in the reciprocal momentum space. An example of a Rashba spin splitting in an inversion-asymmetric nonmagnetic 2D system is illustrated in Fig. 9(a).

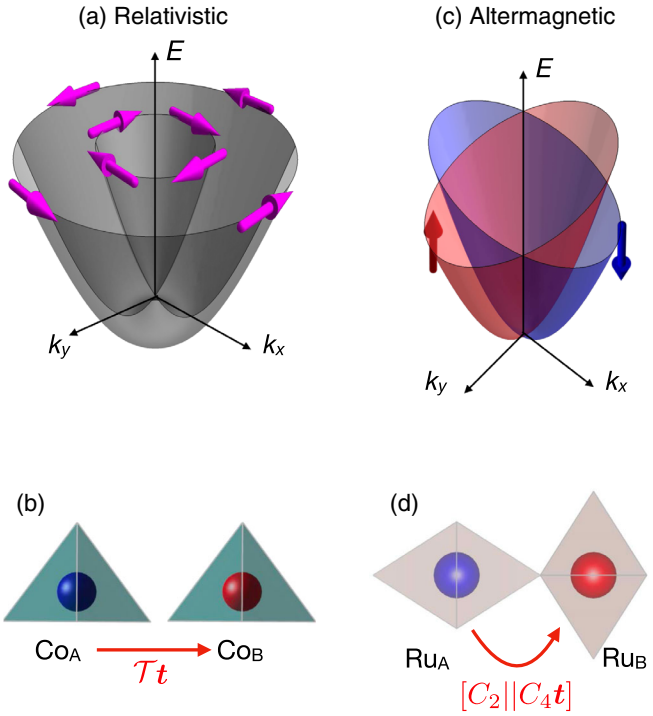

FIG. 9. (a) Model relativistic Rashba spin-split bands. (b) Model of antiferromagnetic zero-magnetization crystal of $BiCoO_3$ with magnetic symmetry $\mathcal{T}\boldsymbol{t}$, and with broken space-inversion symmetry. (c) Model nonrelativistic altermagnetic spin splitting. (d) Model of altermagnetic crystal of RuO_2 with nonrelativistic spin symmetry $[C_2\|C_4\boldsymbol{t}]$. The crystal are discussed in Refs. [16,101].

The second mechanism is associated with $\mathcal{T}$-symmetry breaking by internal magnetization of ferromagnets (ferrimagnets) or by an external magnetic field [62]. Microscopically, the former tends to be dominated by a nonrelativistic magnetic-exchange interaction and is commonly modeled by a momentum-independent effective Zeeman term in the band structure, as illustrated in Fig. 1(a).

Next, we discuss Kramers spin degeneracy in antiferromagnets. All magnetically ordered crystals have broken $\mathcal{T}$ symmetry in the direct space. While this leads to the effective Zeeman spin splitting of the band structure in the reciprocal momentum space in ferromagnets, spin splitting has been commonly considered to be excluded in crystals with a compensating antiparallel arrangement of magnetic moments [1,69–73]. Indeed, there are two types of Kramers spin-degenerate antiferromagnets.

The first type has a symmetry combining $\mathcal{T}$ with translation $\boldsymbol{t}$ in the direct space of the antiferromagnetic crystal. The $\mathcal{T}\boldsymbol{t}$ symmetry defines type-IV magnetic space groups. Among those, only the antiferromagnetic crystals with space-inversion symmetry have the Kramers spin-degenerate bands. As a result, the bands have $\mathcal{T}$ symmetry in the reciprocal momentum space, $\epsilon(s,\mathbf{k}) = \epsilon(-s,-\mathbf{k})$, and inversion symmetry, $\epsilon(s,\mathbf{k}) = \epsilon(s,-\mathbf{k})$, apart from being spin degenerate, $\epsilon(s,\mathbf{k}) = \epsilon(-s,\mathbf{k})$. Examples are FeRh or $MnBi_2Te_4$ [90,91]. In the nonrelativistic limit and for collinear antiferromagnetic order (cf. Sec. II B), the Kramers spin degeneracy is protected by the spin-group symmetry $[C_2\|\boldsymbol{t}]$ alone, i.e., independent of whether the antiferromagnetic crystal is or is not inversion symmetric in the direct space. We note that the nonrelativistic collinear symmetry $[C_2\|\boldsymbol{t}]$ does not imply that all materials described by type-IV magnetic space groups necessarily have vanishing spin splitting in the nonrelativistic limit. This is because type-IV magnetic space groups encompass also noncollinear magnets. However, all materials from type-IV magnetic space groups have $\mathcal{T}$-symmetric bands in the reciprocal space, whether or not relativistic effects are included.

The second type of antiferromagnetic crystals with Kramers spin-degenerate bands break space-inversion and $\mathcal{T}$ (or $\mathcal{T}\boldsymbol{t}$) symmetries in the direct space on their own but have a symmetry in the direct space combining the two transformations. In this case, the Kramers spin-degenerate bands in the reciprocal momentum space have broken inversion symmetry and broken $\mathcal{T}$ symmetry. Here, CuMnAs or Mn_2Au are among the prominent material examples [92–96]. The Kramers spin degeneracy of nonrelativistic bands in the reciprocal space in these collinear antiferromagnets is protected by spin symmetry $[C_2\|\bar{E}]$, in combination with the symmetry $[\bar{C}_2\|\mathcal{T}]$ (cf. second line in Table II). In addition, the $[C_2\|\bar{E}]$ symmetry protects $\mathcal{T}$ symmetry of the nonrelativistic bands, and $[\bar{C}_2\|\mathcal{T}]$ protects inversion symmetry of bands in the nonrelativistic limit. Breaking of inversion symmetry and $\mathcal{T}$ symmetry in the band-structure reciprocal space of this type of collinear antiferromagnets is, therefore, purely of relativistic origin.

To complete the above discussion, we add the following remarks on studies of lifted Kramers spin degeneracy in antiferromagnets. While magnets with compensated magnetic order in the direct space were commonly associated with spin-degenerate bands in the reciprocal momentum space, Zeeman or relativistic spin-splitting mechanisms were also discussed in antiferromagnets. An effective ferromagneticlike Zeeman splitting, and the corresponding $\mathcal{T}$-symmetry breaking in the band-structure reciprocal space, was associated, in antiferromagnets, with a net moment induced by an external magnetic field [97–100]. A $\mathcal{T}$-symmetric relativistic Rashba splitting was predicted in antiferromagnets such as $BiCoO_3$ with broken space-inversion symmetry in the direct space, and with the opposite Co sublattices connected by the real-space $\mathcal{T}\boldsymbol{t}$ symmetry, as shown in Figs. 9(a) and 9(b) [101]. Another example of a magnetic and relativistic splitting was experimentally demonstrated in surface states of antiferromagnetic NdBi [102]. Both of these types of spin splitting offer intriguing interplay with antiferromagnetism. However, they also inherit a net magnetization [Fig. 1(a)] or a noncollinear spin texture [Fig. 9(a)] in the band-structure momentum space, characteristic of conventional ferromagnets or relativistic spin-orbit-coupled systems, respectively.

Having provided the necessary background for contrast, we now discuss the lifting of the Kramers spin degeneracy in the altermagnetic phase. As illustrated in Figs. 9(c) and 9(d), it is principally distinct from the conventional mechanisms. Unlike the relativistic spin-orbit coupling in nonmagnetic (or magnetic) systems, lifting of the Kramers spin degeneracy by altermagnetism does not require breaking of the space-inversion symmetry. In fact, the nonrelativistic band structure of altermagnets has inversion symmetry protected by spin-group symmetry corresponding to the coplanarity of magnetic order, as shown on the second line in Table II. This applies independently of the presence or absence of inversion symmetry in the magnetic crystal structure [16]. Also, unlike the relativistic spin-orbit coupling mechanism, the nonrelativistic electronic states in the altermagnetic bands have a common spin-quantization axis, and spin is a good quantum number. These characteristics are protected by the spin-group symmetry corresponding to the collinearity of magnetic order, as highlighted on the first line in Table II.

Comparing to ferromagnets, altermagnets share the strong nonrelativistic $\mathcal{T}$-symmetry breaking and spin splitting in the band structure. In altermagnets, these characteristics are allowed by the spin-group symmetry shown on the fourth line in Table II. The distinction from ferromagnets is that the same spin-group symmetry also protects the zero nonrelativistic net magnetization in altermagnets.

B. Fermi-liquid instabilities

As discussed in previous sections, altermagnetism can occur in both insulating and metallic systems as a consequence of certain (broken) symmetries of the spin arrangement on the crystal. In this section, we highlight analogies and differences between altermagnetism and the theory of Fermi-liquid instabilities in metallic systems. In Fermi-liquid theory, interactions among electron quasiparticles are described by Landau parameters in spin-singlet and spin-triplet channels, using an orbital angular-momentum partial-wave expansion. Large (negative) values of Landau parameters lead to Pomeranchuk Fermi-liquid instabilities [31,103]. A prominent example of an isotropic s-wave instability in the spin-triplet channel is Stoner ferromagnetism, which corresponds to the momentum-independent effective Zeeman spin splitting in the electronic band structure.

Theoretically, a rich landscape of quantum ordered phases is linked to anisotropic (nonzero angular-momentum) Landau parameters [31]. However, experimental indications of anisotropic Fermi-liquid instabilities are rare: for example, nematic-phase instabilities in the spin-singlet channel with nonzero angular momenta. Their typical characteristics are anisotropic distortions of Fermi surfaces. Nematic instabilities have been considered in fractional quantum Hall systems, Mott insulators, or high-T_c superconductors—all belonging to the family of complex, strongly correlated systems [31].

In analogy to Stoner ferromagnetism, nonzero angular-momentum instabilities in the spin-triplet channel typically break the $SU(2)$ symmetry of the nonrelativistic nonmagnetic Fermi liquid [31]. Altermagnetic symmetries are reminiscent of even-parity wave Fermi-liquid instabilities in the spin-triplet channel [16,18]. Despite the reminiscence, we now illustrate, on the band structure of RuO_2, that the predicted characteristics of the altermagnetic symmetries are extraordinary.

A spin-splitting mechanism due to an anisotropic exchange interaction [13,18,20,21] can be identified in parts of the RuO_2 band structure with a single twofold spin-degenerate band in the nonmagnetic phase, which, in the altermagnetic phase, undergoes an anisotropic, momentum-dependent spin splitting with alternating sign [16]. This is illustrated in Figs. 10(a) and 10(b) on a schematic diagram and *ab initio* bands of RuO_2. Remarkably, the mechanism is dominated by anisotropic exchange interactions; i.e., it persists without including many-body correlation effects beyond the effective single-particle, local-spin-density approximation [16,18].

An effective single-particle, two-band Hamiltonian,

$$H = 2t\cos k_x \cos k_y + 2t_J \sin k_x \sin k_y \sigma_z, \qquad (1)$$

that models this mechanism contains, apart from the common kinetic-energy hopping term, a spin-dependent

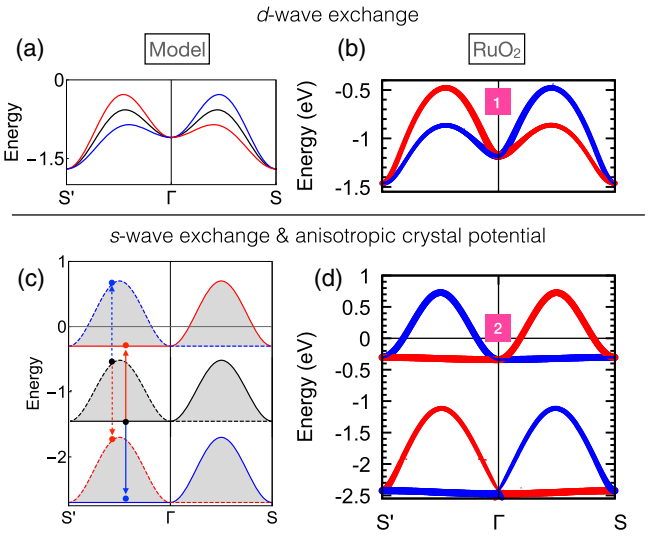

FIG. 10. (a) Schematic diagram of the anisotropic (d-wave) exchange Fermi-liquid instability in the altermagnet. The black line corresponds to the spin-degenerate band in the nonmagnetic phase, while red and blue lines are spin-split bands in the altermagnetic phase. (b) Spin-projected (and orbital-projected) *ab initio* bands of RuO_2 in the energy window corresponding to panel (a). (c) Schematic diagram of the isotropic (s-wave) exchange Fermi-liquid instability combined with anisotropic crystal potential in the altermagnet. Solid and dashed black lines correspond to the spin-degenerate bands dominated by one or the other sublattice in the nonmagnetic phase, respectively. Red and blue lines are spin-split bands in the altermagnetic phase. (d) Spin-projected (and orbital-projected) *ab initio* bands of RuO_2 in the energy window corresponding to panel (c). Pink boxes with labels 1 and 2 correspond to the full *ab initio* bands of RuO_2 shown in Fig. 3(c). This figure is adapted from Ref. [16].

hopping due to the anisotropic exchange interaction in the altermagnetic state [6,7,13]. The model band structure is plotted in Figs. 11(a) and 11(b). The energy spectrum exhibits spin-degenerate nodal surfaces at $k_{x,y} = 0, \pi$, marked in gray in Fig. 11(a), and protected by mirror plane symmetries that transform one spin sublattice on the opposite-spin sublattice and are contained in the little groups of the nodal-surface momenta (cf. fifth line in Table II). The resulting nodal structure and spin-splitting modulation pattern correspond to a d_{xy}-wave symmetry. The characteristic d_{xy}-wave spin-up and spin-down Fermi surfaces are anisotropic and mutually rotated by 90°, following the $[C_2\|C_4]$ spin-group symmetry. *Ab initio* bands of RuO_2 and the corresponding model thus illustrate altermagnetic symmetries reminiscent of a d-wave, spin-triplet, Fermi-liquid instability. However, the d-wave altermagnetism is not ascribed to strong correlations but originates from the (broken) symmetries of the spin arrangement on the crystal.

Remarkably, the *ab initio* band structure of RuO_2 demonstrates an additional, distinct spin-splitting mechanism. In this case, the size and momentum dependence of a

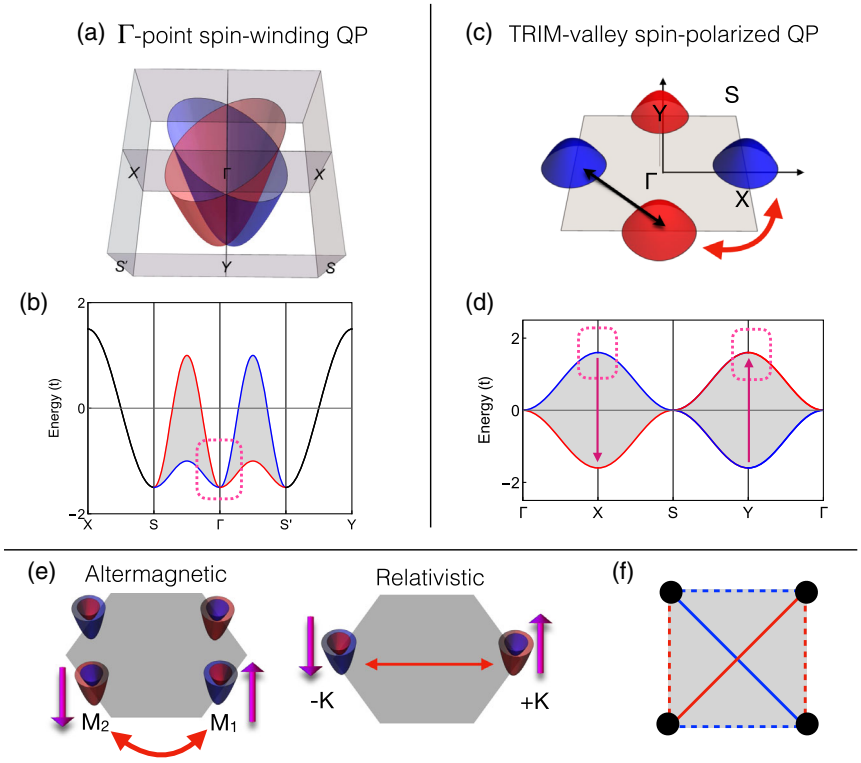

FIG. 11. (a,b) Model of the altermagnetic quasiparticle with quadratic dispersion around the spin-degenerate **Γ** point, and spin-winding number 2 around the **Γ** point. The model corresponds to Eq. (1). (c,d) Model of the altermagnetic spin-polarized valley quasiparticle with no spin winding in the valley. The model corresponds to Eq. (2). The center of a valley is at TRIM, and the spin polarization is opposite at TRIM **X** and **Y**. (e) Schematic illustration of distinct symmetries of band structures with nonrelativistic altermagnetic and relativistic nonmagnetic valleys. (f) Real-space spin-dependent hoppings used to construct model band structures in panels (a)–(c). This figure is adapted from Refs. [6,7,13].

strong nonrelativistic altermagnetic spin splitting is determined by the band splitting due to an anisotropic crystal potential of the nonmagnetic phase [16]. This unconventional electric spin-splitting mechanism is illustrated on a schematic diagram in Fig. 10(c). In the nonmagnetic state, there are two spin-degenerate bands that cross at the fourfold spin and orbital-degenerate **Γ** point, while the orbital degeneracy is lifted away from the **Γ** point. One of the two spin-degenerate bands has a dominant projection on one sublattice, while the other band has a dominant projection on the other sublattice. The bands are anisotropic due to the anisotropy of the crystal potential (cf., third line in Table II). The anisotropies of the spin-degenerate bands corresponding to the two sublattices are mutually rotated by 90°, reflecting the real-space C_4 rotation symmetry that transforms one crystal sublattice on the other. As a result, there is a mutual momentum-dependent splitting between the two spin-degenerate bands away from the **Γ** point in the nonmagnetic phase. Upon the transition to the magnetically ordered altermagnetic phase, an additional momentum-independent (isotropic) exchange interaction occurs, with opposite sign in the bands corresponding to opposite-spin sublattices. As a result, two pairs of spin-split bands form with opposite sign of the spin splitting. For a given pair, the size and momentum dependence of the spin splitting is a copy of the size and momentum dependence of the orbital splitting in the nonmagnetic state. The presence of this microscopic spin-splitting mechanism in RuO_2 is again confirmed by *ab initio* calculations shown in Fig. 10(d). In this case, the altermagnet can be viewed as two interpenetrating *s*-wave Stoner ferromagnets with opposite magnetizations that, because of the interplay with anisotropies of the crystal potential, generate spin-split *d*-wave-like Fermi surfaces.

The potential richness of the landscape of altermagnetism can be further inferred by inspecting the symmetries of all altermagnetic spin groups. Each altermagnetic spin point group can be associated with a given even-parity wave anisotropy of the spin-split Fermi surfaces around the **Γ** point [16]. Apart from the *d*-wave form, this anisotropy can have a *g*-wave or *i*-wave form [16].

Finally, we recall that the discovery of the unconventional *d*-wave superconductivity not only opened an entirely new research landscape of this many-body phase [30] but also raised a fundamental question of whether and how an unconventional *d*-wave counterpart could be realized in magnetism [29]. Earlier considerations focused on possible realizations of the unconventional *d*-wave

magnetism due to strong electronic correlations [31–33]. In contrast, the d-wave (or higher even-parity wave) altermagnetism discussed above is directly linked to symmetries of the effective single-particle crystal potential and does not require strongly correlated systems. This makes the altermagnetic materials discussed in this work realistic candidates for a robust unconventional d-wave (or higher even-parity wave) magnetism, which can host time-reversal symmetry-breaking responses of comparable strength to the conventional s-wave ferromagnets. Moreover, we have already emphasized that the altermagnetic symmetries can equally hold for the Dyson-equation description of correlated systems, as for the effective single-particle Kohn-Sham potentials. Therefore, altermagnets may also facilitate the originally perceived realization of the unconventional d-wave magnetism via strong correlations.

C. Electron quasiparticles

The predicted extraordinary Fermi-liquid instabilities in altermagnets can generate a variety of unconventional electron quasiparticles. An example can be illustrated on the energy bands of the model two-band Hamiltonian (1) in the $\mathbf{k}\cdot\mathbf{p}$ approximation around the $\mathbf{\Gamma}$ point, highlighted by a dashed rectangle in Fig. 11(b). The spin-dependent part of the band structure is given by $2t_J k_x k_y \sigma_z$. The spin degeneracy of the $\mathbf{\Gamma}$ point is generally protected in altermagnets by the spin-group symmetry $[C_2\|A]$ because the $\mathbf{\Gamma}$ point is invariant under any real-space symmetry transformation (including the rotations A). The $\mathbf{\Gamma}$-point spin degeneracy is analogous to the $\mathcal{T}$-symmetric relativistic bands. Here, an example is the Rashba model whose spin-dependent part is given by $\lambda(k_x\sigma_y - k_y\sigma_x)$ [Fig. 9(a)]. However, unlike the linearly dispersing quasiparticles around the $\mathbf{\Gamma}$ point of the inversion-asymmetric relativistic bands, the altermagnetic quasiparticles in the above model have a quadratic dispersion around the $\mathbf{\Gamma}$ point, in line with the general inversion symmetry of bands in altermagnets (cf. second line in Table II).

The altermagnetic quasiparticles are spin polarized away from the $\mathbf{\Gamma}$ point and can be assigned a characteristic even integer, defined as follows [16]: When making a closed loop in the momentum space around the $\mathbf{\Gamma}$ point in a plane orthogonal to a spin-degenerate nodal surface crossing the $\mathbf{\Gamma}$ point, the spin rotates by 360° following two discrete reversals. Each spin-degenerate nodal surface crossing the $\mathbf{\Gamma}$ point, which is present in the crystal momentum space, generates such a spin rotation. The characteristic spin-group integer is defined as the number of these spin-degenerate nodal surfaces crossing the $\mathbf{\Gamma}$ point. It can be 2 (d-wave), 4 (g-wave), or 6 (i-wave) in altermagnets [16]. This illustrates the potential richness of the spin-polarized quasiparticles in altermagnets around the $\mathbf{\Gamma}$ point.

The characteristic spin-group integer of the above altermagnetic quasiparticle model is 2. This is in contrast to the spin-winding number 1 in the relativistic Rashba model. We also point out that the spin-winding number in the relativistic systems is associated with continuously varying spin direction in the momentum space. In contrast, altermagnets show that nonzero integer invariants, describing how many times the quasiparticle spin reverses when completing a closed path around the $\mathbf{\Gamma}$ point, can also exist in systems where all spins share a common spin quantization axis, and spin is a good quantum number.

A different type of predicted altermagnetic electron quasiparticle can be illustrated on a two-band model Hamiltonian [6,7,13]:

$$H = \pm 2t_J(\cos k_x - \cos k_y)\sigma_z, \tag{2}$$

whose energy spectrum is shown in Fig. 11(d). [Around the Γ point, Eq. (2) is related to the model in Eq. (1) by a 45° rotation of the momentum space, and by setting $t = 0$.]

In the $\mathbf{k}\cdot\mathbf{p}$ approximation around time-reversal invariant momenta (TRIMs) $\mathbf{X}$ and $\mathbf{Y}$, highlighted by dashed rectangles in Fig. 11(d), the spectrum takes the form of spin-split valleys given by [see Figs. 11(c) and 11(d)],

$$\begin{aligned} E_\pm(\mathbf{X},\mathbf{k}) &= \pm t_J(4-k^2), \\ E_\pm(\mathbf{Y},\mathbf{k}) &= \mp\, t_J(4-k^2). \end{aligned} \tag{3}$$

(Recall that a momentum $\mathbf{k}$ is time-reversal invariant when it differs from $-\mathbf{k}$ by a reciprocal lattice vector.)

The possibility to observe spin-split valleys around TRIMs in real materials is predicted by the spin-group symmetry analysis and *ab initio* band-structure calculations of the altermagnetic phase in, e.g., Mn_5Si_3 [6] [Fig. 7(c)]. Besides 3D crystals, the altermagnetically spin-split valleys can also form in 2D materials [15,23,104], as predicted, e.g., in *ab initio* calculations of the band structure of a monolayer insulator V_2Se_2O [15] [Fig. 7(d)].

Locally, the individual valleys around the $\mathbf{X}$ and $\mathbf{Y}$ TRIMs are isotropic in the above model. This illustrates that altermagnets can host spin-polarized quasiparticles analogous to the model nonrelativistic s-wave Stoner ferromagnet, with no spin winding around the TRIM. However, unlike ferromagnets, the altermagnetic spin-group symmetries impose that each spin-split TRIM has a counterpart TRIM elsewhere in the Brillouin zone with opposite spin splitting. The presence of these TRIM pairs is protected by the $[C_2\|A\mathbf{H}]$ spin-group symmetries (cf. fourth line in Table II).

The altermagnetic spin-polarized quasiparticles in separate local valleys in the momentum space are reminiscent of relativistic spin-polarized valley quasiparticles in nonmagnetic hexagonal 2D materials, such as transition metal dichalcogenides [105]. The common features shared by the altermagnetic and relativistic quasiparticles are the opposite spin polarization in valleys occupying different parts of the Brillouin zone, and the zero net spin polarization when

integrated over the whole Brillouin zone. However, only altermagnets allow these valleys to be centered at TRIMs, as highlighted in Fig. 11(e). In the nonmagnetic relativistic systems, spin splitting is excluded by $\mathcal{T}$ symmetry not only at the $\mathbf{\Gamma}$ point but at all TRIMs.

So far, we have discussed the electron quasiparticles from the symmetry perspective limited to the spin-group transformations acting on the spin- and momentum-dependent band structure. Additional, rich, quasiparticle physics, including higher-order degeneracy quasiparticles, can emerge from the analysis of spin-group transformations acting on the electron wave functions (spin-group representations) [16,24,59,61].

D. Magnons

Besides the electron energy spectra and quasiparticles, we foresee that the symmetries of the direct-space spin-polarization order parameter in altermagnets will also be reflected in unconventional characteristics in the reciprocal momentum space of the spin-wave spectra and magnon quasiparticles [106].

The typically leading contribution to the magnon spectra can be obtained by mapping the spin-dependent electronic structure on the Heisenberg Hamiltonian, $H = -\sum_{i\neq j} J_{ij}\hat{\mathbf{e}}_i\hat{\mathbf{e}}_j$ [59,107,108]. Here, $\hat{\mathbf{e}}_i$ is the direction of the magnetic moment around an atom at position R_i, and J_{ij} are Heisenberg exchange coupling parameters. In the Heisenberg model, the real- and spin-space transformations are decoupled, and the symmetries of the corresponding magnon bands can be described by the nonrelativistic spin-group formalism [26,59].

In antiferromagnets, translation or inversion symmetry transformations connecting opposite-spin sublattices protect the degeneracy of opposite-chirality magnon bands [26,59]. This has been commonly illustrated on the opposite-spin sublattices of rutile crystals while omitting the presence of nonmagnetic atoms in these crystals [26,59,109]. We have seen in Sec. II, however, that the nonmagnetic O atoms in metallic rutile RuO_2, or F atoms in insulating rutiles FeF_2 or MnF_2, break the translation and inversion symmetries connecting the opposite-spin sublattices. Instead of classic antiferromagnets [26,49,59,109], rutiles are the prototypical representatives of d-wave altermagnetism [16], with interlinked unconventional properties of the direct-space crystal structure and reciprocal-space electronic, as well as magnonic, band structure [106]. Hematite Fe_2O_3 is another prominent insulating compensated magnet in magnonic research [110]. In analogy to the rutiles, the nonmagnetic O atoms in Fe_2O_3 break the translation and inversion symmetries while preserving a rotation symmetry, connecting the opposite-spin sublattices. Fe_2O_3 is an example of a g-wave altermagnet [16].

In analogy to the electronic band structure, the degeneracy of magnon bands with opposite chirality is predicted to be lifted in altermagnets, with the sign of the splitting alternating across the magnon Brillouin zone [106]. On one hand, altermagnetic magnons can be chiral and carry spin currents, similar to ferromagnets but with highly anisotropic characteristics. On the other hand, the dispersion of altermagnetic magnons can be linear around the degenerate $\mathbf{\Gamma}$ point, similar to antiferromagnets.

For metallic systems, the Landau damping in altermagnets can be suppressed due to the spin splitting of the electron quasiparticles. This is more reminiscent of the low Landau damping in metallic ferromagnets and contrasts with the large Landau damping associated with the spin degeneracy of the electronic bands in antiferromagnets [106,108]. All these unconventional characteristics make altermagnets a promising material platform for magnonics, including the exploration and exploitation of the emission, propagation, and detection of ultrashort (ps-scale) THz magnon pulses of wavelengths orders of magnitude smaller than the wavelengths of the THz photons.

E. Berry phase, nondissipative transport, and band topology

The Berry phase is a general concept in quantum mechanics [111]. A prototypical example is the Aharonov-Bohm phase given by a real-space path integral of the electrodynamic vector potential along a closed loop or, equivalently, by an integral of the magnetic field over an area enclosed by the loop. The phase can be macroscopically observable by resistance oscillations in an applied magnetic field.

In the crystal momentum space, a Berry connection analogue of the electrodynamic vector potential, and a Berry curvature analogue of the magnetic field,

$$\begin{aligned}\boldsymbol{\mathcal{A}}_n(\mathbf{k}) &= i\langle u_{n\mathbf{k}}|\nabla_{\mathbf{k}}u_{n\mathbf{k}}\rangle,\\ \boldsymbol{\mathcal{B}}_n(\mathbf{k}) &= \nabla_{\mathbf{k}}\times\boldsymbol{\mathcal{A}}_n(\mathbf{k}),\end{aligned} \tag{4}$$

can also generate macroscopic observables. A prominent example is the nondissipative Hall current given by the transverse conductivity [37],

$$\sigma_{xy}^{\mathrm{Hall}} = -\frac{e^2}{\hbar}\sum_n \int_{\mathrm{BZ}} \frac{d^3k}{(2\pi)^3} f[\varepsilon_n(\mathbf{k})]\mathcal{B}_n^z(\mathbf{k}). \tag{5}$$

Here, $f[\varepsilon_n(\mathbf{k})]$ is the Fermi-Dirac distribution function, $\varepsilon_n(\mathbf{k})$ is the energy of the Bloch state in band n with crystal momentum $\mathbf{k}$, and $u_{n\mathbf{k}}(\mathbf{r})$ is the periodic part of the Bloch wave function.

Altermagnets are predicted to bring unique elements into the physics of Berry phase phenomena [2,3,5–7,44,45]. The Berry curvature near the $\mathbf{\Gamma}$ point of a $\mathbf{k}\cdot\mathbf{p}$ altermagnet-Rashba model [2], $tk^2 + 2t_J k_x k_y \sigma_z + \lambda(k_x\sigma_y - k_y\sigma_x)$, is given by

$$\mathcal{B}(k)_{\pm} = \mp \frac{2t_J\lambda^2 k_x k_y}{\sqrt{4t_J^2(k_x k_y)^2 + \lambda^2 k^2}}. \quad (6)$$

Equation (6) illustrates that the characteristic even-parity wave (e.g., d-wave) anisotropy in the nonrelativistic band structure of altermagnets can also be reflected in their relativistic Berry curvature. In contrast, a counterpart ferromagnet-Rashba model, $tk^2 + \Delta\sigma_z + \lambda(k_x\sigma_y - k_y\sigma_x)$, gives an isotropic Berry curvature near the $\mathbf{\Gamma}$ point [2,37,112–115], reflecting the principally isotropic s-wave nature of ferromagnetism.

The Berry curvature tends to reach the highest values near band (anti)crossings [2,37], which implies another outstanding feature of altermagnets. In contrast to the typically accidental (anti)crossings in ferromagnets, the spin-group symmetries of altermagnets impose the presence of the spin-degenerate nodal surfaces in the nonrelativistic band structure (cf. fifth line in Table II). When the relativistic spin-orbit coupling is included, these nodal surfaces (which may be weakly gapped by the spin-orbit coupling) may become symmetry-defined Berry-curvature hotspots. This is illustrated in Fig. 5 on relativistic *ab initio* band structures of RuO_2 and $FeSb_2$ [2,7,13].

Since $\mathcal{T}$ is antiunitary in quantum mechanics, the Berry curvature (4) is odd under $\mathcal{T}$, $\mathcal{T}\boldsymbol{\mathcal{B}}_n(\mathbf{k}) = -\boldsymbol{\mathcal{B}}_n(-\mathbf{k})$, implying that the integral in Eq. (5) vanishes in $\mathcal{T}$-symmetric band structures. Breaking of $\mathcal{T}$ symmetry in the band structure of altermagnets is, therefore, the key property that allows for the observation of macroscopic responses, such as the anomalous Hall effect [2,3]. Recent experiments [5] have detected the anomalous Hall effect in RuO_2 of a comparable strength to typical Hall signals in ferromagnets. This is consistent with the predicted strong altermagnetic $\mathcal{T}$-symmetry breaking in the band structure of this compensated collinear magnet [3,5] (cf. Table I).

RuO_2 is an example in which the lattice of the magnetic Ru atoms alone would have the opposite-spin sublattices connected by a translation. As mentioned above, this symmetry would imply $\mathcal{T}$ symmetry of the band structure (and in combination with inversion symmetry of the crystal, also spin degeneracy). The presence of the nonmagnetic oxygen atoms is, therefore, essential for the $\mathcal{T}$-symmetry breaking (and spin splitting) in the altermagnetic band structure of RuO_2 and, consequently, for the anomalous Hall effect [3]. The term "crystal Hall effect" [3,7,44,117] was introduced to highlight this feature. One of the implications, unparalleled in the conventional anomalous Hall effect in ferromagnets, is that in altermagnets the Hall signal is predicted to flip sign not only when reversing the magnetic moments but also when the symmetry-breaking arrangement of nonmagnetic atoms reverses between the two magnetic sublattices [3].

Next, we recall that in 2D systems, Eq. (5) turns into a surface integral proportional to the Berry phase, which becomes quantized when the integration covers the full Brillouin zone in 2D insulators [118]. The corresponding quantum Hall effect [119] was demonstrated in graphene at room temperature [120], but it requires a strong magnetic field. The ferromagnetic quantum anomalous Hall counterpart [121] can be observed at zero magnetic field but, so far, has been limited to Kelvin temperatures [42,122]. Since altermagnetism can host the Berry phase phenomena and can occur in 2D crystals and in insulators, it opens new possibilities in the search for high-temperature zero-field quantum Hall phenomena. For a further in-depth discussion of Berry phase physics and nondissipative Hall transport in altermagnets, we refer to the recent topical review [2].

While above we have discussed topological Berry phase physics, which is a consequence of perturbative relativistic spin-orbit coupling effects, altermagnets can also lead to identification of unconventional magnetic topologies of a nonrelativistic origin [7,16]. The spin degeneracies in nonrelativistic altermagnetic bands are protected by symmetries of the spin point group (spin Laue group) because the electronic structure is strictly separated into nonmixing spin-up and spin-down channels [16]. However, additional band degeneracies can exist within one spin channel, i.e., degeneracies in band indices other than spin, which are protected by space-group symmetries (symmetry transformations also containing translations). These features can be included in the symmetry analysis based on the nonrelativistic spin-group formalism and can be important when exploring exotic topological quasiparticles near such degeneracies [16,24,25,57,58]. The nonrelativistic spin-space groups are also well suited for exploring magnon band topology [59] of altermagnets.

IV. RESEARCH AREAS

We now move to the discussion of the potential of altermagnetism in specific areas of condensed-matter research. We start from spintronics in which, besides the anomalous Hall effect, initial theory predictions of nonrelativistic spin-dependent responses have recently been tested by experiments.

A. Spintronics

To highlight the novelty of the emerging concept of spintronics without magnetization and relativity, enabled by altermagnetism, we first briefly recall the principles of the established fields of spintronics in ferromagnets and antiferromagnets.

The nonrelativistic electronic structure of ferromagnets is split into majority and minority spin bands that break the $\mathcal{T}$ symmetry and where spin is a good quantum number independent of momentum. This results in different conductances of the two conserved spin channels, which makes electrical currents in ferromagnets strongly spin polarized. Passing the spin-polarized current in a multilayer structure

with reference and sensing (or recording), ferromagnetic electrodes can generate spin-transfer torque (STT) and giant/tunneling magnetoresistance (GMR/TMR) effects. These strong nonrelativistic responses facilitate reorientation between parallel and antiparallel magnetizations of the two ferromagnetic electrodes and corresponding resistive changes on a scale of around 10%–100% utilized in commercial spintronic memory devices [85–87,123].

Direct antiferromagnetic counterparts of STT and GMR/TMR effects are principally excluded by the $\mathcal{T}$ invariance and spin degeneracy of the nonrelativistic electronic structure. As a result, the research of antiferromagnetic spintronics turned to the typically weaker relativistic phenomena, such as the spin-orbit torque reorientation of the Néel vector detected by a scale of about 0.1%–1% anisotropic magnetoresistance [39,40,92,93,124]. The concept inherits the general weakness of relativistic spintronic phenomena that are simultaneously generated and suppressed by the spin nonconserving nature of the relativistic spin-orbit coupling [40].

The strong nonrelativistic $\mathcal{T}$-symmetry breaking and spin splitting in altermagnetic bands directly opens a possibility to not only replicate the concepts known from ferromagnets but also to enrich nonrelativistic spintronics by new effects and functionalities linked to the zero nonrelativistic net magnetization [4,8–15].

The anisotropy of the split and equally populated spin-up and spin-down Fermi surfaces in altermagnets [cf. Figs. 11(a) and 11(b)] results in spin-dependent anisotropic group velocities, $\partial E_+(\mathbf{k})/\partial k_i \neq \partial E_-(\mathbf{k})/\partial k_i$, where $+/-$ refers to the spin index. The corresponding conductivities in d-wave altermagnets are then also spin dependent and anisotropic. Considering the x and y directions as the anisotropic axes of the spin-split Fermi surfaces, we get $\sigma_{+,xx} \neq \sigma_{-,xx}$, $\sigma_{+,yy} \neq \sigma_{-,yy}$, and $\sigma_{\pm,xx} = \sigma_{\mp,yy}$. The electrical current then becomes spin polarized when the bias is applied along the x or y direction, as schematically illustrated in Fig. 12(a). Moreover, as a consequence of the $\mathcal{T}$-symmetry breaking of the spin-split bands, the sign of the spin polarization reverses when reversing the altermagnetic-order vector. (In analogy to the antiferromagnetic Néel vector, we define the altermagnetic-order vector as the difference between the magnetization vectors of the opposite-spin sublattices.)

The above nonrelativistic spin-current characteristics are analogous to ferromagnets. However, in contrast to ferromagnets, the altermagnetic spin splitting is also predicted to cause the reversal of the spin polarization of the current when the applied electrical bias is flipped between the x and y directions.

The spin-polarized current directly implies a GMR effect in a stack comprising two altermagnets, separated by a conductive nonmagnetic spacer, with the altermagnetic-order vectors oriented either parallel or antiparallel, as illustrated in Fig. 12(b). The contribution to GMR from the spin-dependent conductivities in d-wave altermagnets can be estimated from the conventional current-in-plane GMR expression derived in ferromagnets [85],

$$\mathrm{GMR} = \frac{1}{4}\left(R_\sigma + \frac{1}{R_\sigma} - 2\right), \tag{7}$$

where $R_\sigma = \sigma_{+,xx}/\sigma_{-,xx} = \sigma_{+,xx}/\sigma_{+,yy} = \sigma_{-,yy}/\sigma_{-,xx}$. The *ab initio* calculations in RuO_2 give GMR reaching a 100% scale [13] [Fig. 12(e)], highlighting the expected large GMR ratios in altermagnets.

As noted above, the polarization of the longitudinal spin-polarized current in altermagnets is predicted to reverse not only with the reversal of the altermagnetic-order vector but also with the reorientation (e.g., by 90°) of the applied electrical bias in the d-wave altermagnet. A directly related effect, also unparalleled in ferromagnets, is illustrated in Fig. 12(c). For a bias applied in the diagonal direction between the two anisotropy axes of the spin-split Fermi surfaces, the longitudinal current is unpolarized. However, a nonrelativistic spin current is generated in the transverse direction. The effect has been predicted in a range of inorganic and organic materials [4,8,9,15]. The d-wave altermagnet acts here as an electrical spin splitter, with a propagation angle between spin-up and spin-down currents reaching 34° in RuO_2 [8]. The corresponding charge-spin conversion ratio reaches a remarkable 28% [Fig. 12(e)], and the spin conductivity is a factor of 3 larger than the record value from a survey of 20 000 nonmagnetic relativistic spin-Hall materials [125].

The above outstanding charge-spin conversion efficiency of altermagnetic RuO_2 prompted a theoretical proposal of a spin-splitter torque (SST) [8], in part already supported by initial experiments [10–12] (cf. Table I). In the geometry schematically illustrated in Fig. 12(d), an in-plane bias generates the nonrelativistic spin current in the d-wave altermagnetic film along the out-of-plane direction, with the polarization of the spin current controlled by the orientation of the altermagnetic-order vector. The spin current then exerts a torque on the adjacent altermagnetic (or ferromagnetic) layer. SST does not inherit the problems of STT associated with the out-of-plane direction of the applied electrical bias [86,126]. Instead, it shares the in-plane electrical-bias geometry of the spin-orbit torque generated by the relativistic spin-Hall polarizer while circumventing the limitations of the more subtle relativistic spintronic effects [40].

Another nonrelativistic spintronic effect that can be generally expected to exist in altermagnets is a variant of the TMR in a tunnel junction with an insulating spacer separating the two altermagnetic electrodes [13,14]. The altermagnetic TMR can be illustrated on the model band structure with spin-split valleys [cf. Figs. 11(c) and 11(d)]. The pairs of valleys with opposite spin polarization result in the equal net population of spin-up and spin-down states,

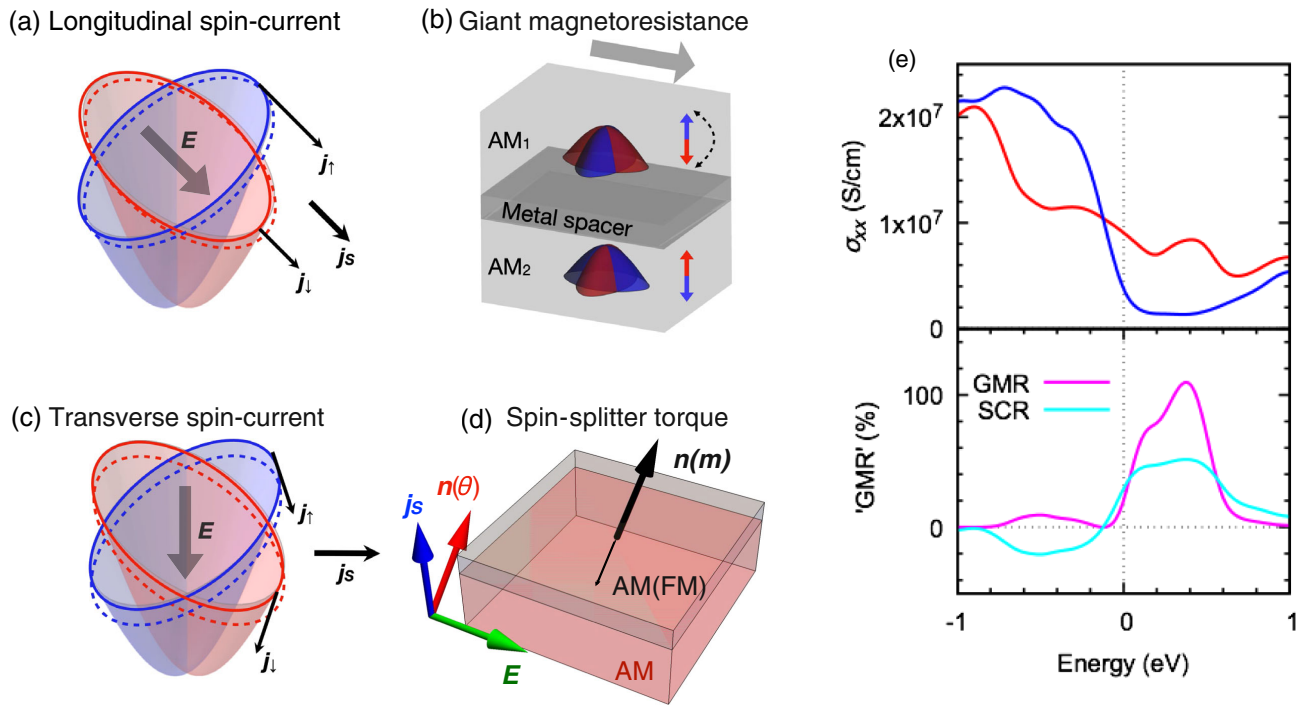

FIG. 12. (a) Schematics of the longitudinal spin current in altermagnets. For an electric bias **E** applied along one of the main anisotropy axes of the spin-split Fermi surfaces, the spin-up and spin-down charge currents are parallel but of different magnitudes due to the Fermi-surface anisotropies. As a result, the longitudinal charge current is spin polarized. (b) Schematics of a GMR stack in a current-in-plane geometry. As an example, we show the antiparallel configuration of the altermagnetic-order vectors in the two electrodes AM_1 and AM_2. Interfaces are oriented along one of the main anisotropy axes of the spin-split bands. Energy band cuts highlight the anisotropy around the **Γ** point, resulting in anisotropic spin-dependent conductivities. (c) Schematics of the transverse spin current. For **E** applied in the diagonal direction between the two anisotropy axes of the spin-split Fermi surfaces, the spin-up and spin-down charge currents combine in an unpolarized longitudinal charge current and in a pure transverse spin current. (d) Spin-splitter-torque concept on a schematic of altermagnetic-altermagnetic (ferromagnetic) bilayer. A spin-current from the bottom altermagnet propagates in the out-of-plane direction and generates a spin-splitter torque on the altermagnetic (or ferromagnetic) order vector in the top layer. (e) *Ab initio* longitudinal spin-up and spin-down conductivities (red and blue), GMR, and the ratio of the transverse spin current relative to the longitudinal charge current (SCR) in RuO_2. This figure is adapted from Refs. [8,13].

while the densities of states within a given valley become spin dependent, $n_+(\mathbf{M}_1) \neq n_-(\mathbf{M}_1)$, $n_+(\mathbf{M}_2) \neq n_-(\mathbf{M}_2)$, and $n_\pm(\mathbf{M}_1) = n_\mp(\mathbf{M}_2)$. For tunneling that conserves the valley index, parallel and antiparallel configurations of altermagnetic-order vectors in the two layers, illustrated in Fig. 13(a), are predicted to give different conductances, in analogy to ferromagnetic TMR. This can be seen by applying the Jullière formula [85] per valley [13],

$$\mathrm{TMR} = \frac{1}{2}\left(R_n + \frac{1}{R_n} - 2\right), \tag{8}$$

where the ratio of the spin-up and spin-down densities of states in the valley is given by $R_n = n_+(\mathbf{M}_1)/n_-(\mathbf{M}_1) = n_+(\mathbf{M}_1)/n_+(\mathbf{M}_2) = n_-(\mathbf{M}_2)/n_-(\mathbf{M}_1)$.

The *ab initio* calculations of about 100% TMR ratios in RuO_2 [Fig. 13(b)] or Mn_5Si_3 [13,14] illustrate the potential for achieving large TMR responses in tunnel junctions with altermagnetic electrodes.

Finally, we note that symmetry-wise, TMR is, in principle, expected in all altermagnetic spin groups [13] and can reach large magnitudes as long as the spin-polarized quasiparticles are well separated in the momentum space to provide for the sufficiently decoupled spin transport channels [Fig. 13(c)]. On the other hand, the GMR derived from the anisotropy of the macroscopic (averaged over momentum) spin-dependent conductivities is predicted to be allowed only in *d*-wave altermagnets [13,16].

We now proceed to the discussion of how altermagnetism can contribute to the research of space, time, and energy downscaling in spintronic devices. The nonrelativistic nature and corresponding large strength of the GMR (TMR) and SST (STT) effects are important prerequisites for temporal and spatial scalability of memory devices utilizing these phenomena for reading and writing information. This highlights the importance of the presence of these phenomena in altermagnets. In contrast, the

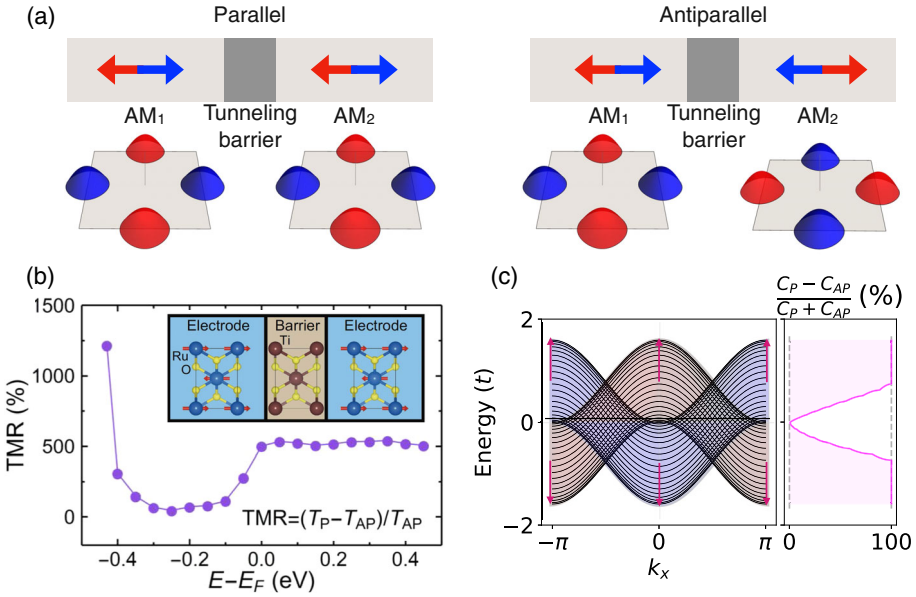

FIG. 13. (a) Schematics of a TMR stack with an insulating barrier and altermagnetic electrodes with parallel and antiparallel order vectors. Energy band cuts highlight the oppositely split valleys, resulting in valley and spin-dependent densities of states. (b) *Ab initio* quantum-transmission calculations of the TMR in a RuO_2| TiO_2| RuO_2 tunnel junction. (c) Model spin and transport-momentum projected band structure, and relative difference between the conductances in the parallel and antiparallel configurations of the altermagnetic-order vectors in the two electrodes. The TMR is maximized for transport energies corresponding to the spin-split valleys well separated in momentum. This figure is adapted from Refs. [13,14].

scalability is limited in antiferromagnetic devices that rely on the typically weaker relativistic spintronic phenomena.

Realizing the strong nonrelativistic effects and functionalities in altermagnets will bring advantages compared to antiferromagnets and to ferromagnets. The large nonrelativistic magnetization, accompanying the spin-polarized band structure of ferromagnets, represents a significant limitation for spintronics. The low tolerance to perturbing magnetic fields implies that stray magnetic fields from the ferromagnetic films in the GMR(TMR)/STT stacks have to be suppressed by elaborate device engineering to eliminate magnetic cross-talk within and between individual memory bits. This is achieved at the expense of synthesizing complex multilayer stacks, with typically over ten different materials, in which the reference or recording electrodes comprise two or more ferromagnetic layers with mutually compensating antiparallel magnetizations (the so-called synthetic antiferromagnets) [85,127]. Even in these elaborate multilayers, the net magnetic stray fields can only be partially eliminated. In contrast, altermagnetic crystals with vanishing magnetization and stray fields will offer a magnetic robustness combined with the absence of magnetic cross-talk, which will allow for a significant simplification of the structure of spintronic devices. In combination with the strong GMR (TMR) and SST (STT) effects, this can enable spatial downscaling beyond the limits of ferromagnetic devices.

Another principal advantage compared to ferromagnets, which altermagnets share with antiferromagnets, is the close-to THz range of the resonance frequency of collective spin excitations (magnons), corresponding to the close-to ps internal timescale of spin dynamics. This opens the possibility for achieving the least-dissipative and fastest control of a bistable memory bit [128]. According to the Landauer thermodynamic principle [129,130], confirmed in magnetic systems at above around μs timescales [131,132], the minimal energy dissipation when restoring one memory bit is given by $k_B T \ln 2$, where T is the temperature and k_B denotes the Boltzmann constant. At room temperature, this Landauer limit is in the range of about meV; i.e., it corresponds to the energy of a photon of about THz. Remarkably, switching by an energy corresponding to a single THz photon per magnetic atom, i.e., around meV per atom, and with the limiting ps duration of the delivered THz pulse has been demonstrated recently in a compensated collinear magnet $TmFeO_3$ [128]. This shows that reaching the Landauer energy limit of about meV per memory bit at the limiting ps timescale is becoming a legitimate, albeit still very challenging, research goal in ultrafast photomagnetism [133]. Since the orthoferrite $TmFeO_3$ is an insulating d-wave altermagnet, it also opens the possibility for detecting the ultrafast switching dynamics of the altermagnetic-order vector by the $\mathcal{T}$-symmetry breaking magneto-optical responses commonly employed in ferromagnets. In metallic altermagnets, the research towards the limiting energy and timescales can further benefit from the presence of the strong nonrelativistic GMR (TMR) and SST (STT) responses.

So far, we have discussed concepts of spintronic devices in which the magnetic-order vector is uniformly switched across a manmade memory element. Alternatively, information can be coded in self-assembled magnetic nano-textures, such as domain walls. This is another research area for which the stray-field-free compensated magnets, and altermagnets in particular, can be highly favorable.

Self-assembled magnetic nano-textures in Kramers spin-degenerate antiferromagnets have been suggested as the origin of the recently observed, highly reproducible, analog time-dependent switching over the full range from ms electrical writing pulses to sub-ps optical pulses, and with a resistivity increase in the switched state on a 10%–100% scale [134,135]. The devices mimic a logic-in-memory functionality of spiking neuromorphic elements, thus offering additional space, time, and energy downscaling prospects unparalleled in the conventional digital devices with logic and memory separated by the von Neumann bottleneck. The resistivity increase in the switched state was ascribed to the formation of atomically sharp domain walls [134–136]. They correspond to the ultimate downscaling of a magnetic domain-wall width since the Néel vector flips by 180° from one to the neighboring atomic plane [136]. If generated in an altermagnet, each atomically sharp domain wall separating domains with opposite sign of the altermagnetic-order vector would represent a local GMR junction that is self-assembled and corresponds to the ultimate downscaling of the width of the junction spacer. This atomic-scale GMR would generate a strong additional contribution to the resistances of the atomically sharp domain walls in altermagnets. The altermagnetic phase thus offers a possibility to combine, in one physical system, the phenomena and functionalities of the commercial digital ferromagnetic memory devices and of the experimental antiferromagnetic analog neuromorphic devices.

B. Spin caloritronics, field-effect electronics, and multiferroics

The key merit of ferromagnets from an energy-saving perspective is nonvolatility; i.e., they can store information even when the power is switched off. On the other hand, electrical reading and especially writing information into ferromagnetic memory devices can generate significant Joule heating [85]. This can be directly harvested during the writing process in which the elevated temperature effectively reduces the equilibrium energy barrier separating the states with opposite magnetization orientation. In the latest generation of hard disks, elevating the temperature of a bit while recording is provided through an external laser heat source. Similarly, all-optical switching by laser pulses is typically accompanied by significant heating effects [137]. This brings us to a discussion of how altermagnetism, rather than generating heat, can contribute to energy harvesting in devices combining heat, charge, and spin phenomena.

Ferromagnets have been considered for a direct heat conversion to electricity [138]. Here, the anomalous Nernst effect, a thermo-electric counterpart of the anomalous Hall effect, is regarded as an attractive candidate phenomenon [139]. The anomalous Nernst effect generates an electric field in a transverse direction to the thermal gradient. Particularly in thin-film or nanostructured heat-charge conversion devices, the transverse geometry can significantly enhance the conversion efficiency compared to the conventional longitudinal Seebeck effect [139]. A complementary research area to the anomalous Nernst effect are thermal counterparts of the GMR/TMR and STT phenomena. Here, the energy harvesting concept is based on employing heat gradients, instead of electrical bias, to directly read or write information in a memory device [138].

Altermagnets significantly enlarge the material landscape for realizing and optimizing these thermo-electric responses that originate, in analogy to their electronic counterparts, from the $\mathcal{T}$-symmetry-broken spin-polarized band structure. Unlike the typically metallic ferromagnets, altermagnets are predicted to span a broad range of conduction types (cf. Sec. II D). This prediction is favorable because, from a general thermo-electric perspective, semimetals or semiconductors are more suitable material types than metals due to the strong dependence of their electronic structure on energy near the Fermi level. A particularly intriguing class of materials are those exhibiting a metal-insulator transition. Among the altermagnetic candidate materials, $FeSb_2$ [7,16] is an example in which earlier studies reported an extraordinary (spin-independent) thermo-electric response, linked to the metal-insulator transition [140].

So far, we have discussed electrical-current (voltage) responses to the applied thermal gradients. Altermagnets may also open intriguing new directions in research and application of spin-current responses to thermal gradients in the field commonly referred to as spin caloritronics [138]. In analogy to the anomalous Nernst and Hall effects, there is also a spin Nernst effect [141], driven by a thermal bias, that is a counterpart of the spin Hall effect [38], driven by an electrical bias. Conventionally, these transverse spin-current responses to the applied thermal or electrical bias did not require a magnetically ordered system and were ascribed to the relativistic spin-orbit coupling. As a result of the relativistic origin, their magnitudes were typically weak. In contrast, the transverse spin-current response in altermagnets can be expected to have a strong nonrelativistic contribution, exceeding, by orders of magnitude, the relativistic spin Nernst contribution. The expectation is based on the analogy with the electrically generated transverse spin current discussed earlier in Sec. IV A. In RuO_2, *ab initio* calculations have shown that the electrically induced transverse spin current can have a nonrelativistic contribution, the so-called spin-splitter effect,

which is orders of magnitude stronger than the relativistic spin Hall effect in the same altermagnetic material [8].

As a final remark on spin caloritronics, we recall the spin magnon Nernst effect [142], where, instead of electrons, the spin current is carried by magnons. In Sec. III D, we have highlighted the expected unconventional phenomenology of magnons in altermagnets. Their unparalleled combination of linear dispersion and alternating chirality splitting in the magnon Brillouin zone is potentially highly favorable for realizing spin-caloritronic devices.

Similar to spin caloritronics, nonmetallic materials are also favorable for combining spin physics with field-effect electronics. Earlier research demonstrated the intriguing interplay of spintronic and transistor functionalities in ferromagnetic semiconductors [143,144]. However, the field suffered from the notorious incompatibility of robust high-temperature ferromagnetism with semiconducting band structures. Altermagnets thus open a new prospect of materials with high magnetic transition temperatures, allowing us to combine spintronic and semiconducting device functionalities. The initial experimental demonstration of a spontaneous anomalous Hall effect in the absence of an external magnetic field has been reported in a room-temperature g-wave altermagnetic semiconductor MnTe [145]. Moreover, theory predicts a high sensitivity of this and other spintronic responses to small changes of the Fermi level position near the valence or conduction band edge, which can be controlled by doping or electrostatic gating [145].

Finally, we discuss the prospect of an interplay of altermagnetism with dielectric and ferroelectric (ferroelastic) materials or phases. The initial measurements of the anomalous Hall effect and spin currents in the d-wave altermagnet RuO_2 exploited the high structural compatibility with TiO_2 [5,10,12], which is one of the most commonly used dielectrics in consumer electronics, as well as a commonly employed memristive element in experimental neuromorphic devices [146]. Another closely related dielectric, HfO_2, plays an important role in modern CMOS devices, and the recent discovery of ferroelectricity in HfO_2 thin films has triggered a renewed interest in the development of scalable, nonvolatile, ferroelectric memories [147]. Interfaces of structurally compatible altermagnetic and ferroelectric (ferroelastic) films pave the way for nonvolatile electric-field control of magnetism via a coupling between the ferroic orders. Such a coupling can also be realized in multiferroic materials hosting the magnetic and ferroelectric orders within the same crystal [148]. Since only insulating (semiconducting) materials can be ferroelectric, a coexisting ferromagnetic order is rare because ferromagnetism favors metallic structures, which again highlights the new opportunities brought up by altermagnetism. The prominent multiferroic materials are noncentrosymmetric perovskite oxides with a compensated magnetic order [148]. As shown in Sec. II D, altermagnetism is compatible with this material family. Here, $CaMnO_3$ is an example multiferroic [149] that is a candidate for hosting the d-wave altermagnetic phase [16].

C. Superconductivity

The family of insulating perovskite oxides brings us to its prominent cuprate member La_2CuO_4 that, upon doping, turns into a high-temperature d-wave superconductor [30]. The recognition that this cuprate crystal belongs to a d-wave altermagnetic spin group [16] leads to the anticipation of a new research direction exploring an interplay between altermagnetism and superconductivity [16,150]. Research in this context may include areas such as the coexistence of altermagnetism and unconventional superconductivity with anisotropic Cooper pairing [151], altermagnetic fluctuations as a pairing mechanism [151], or phenomena at altermagnet or superconductor interfaces [152,153].

Since altermagnets have spin-degenerate nodal surfaces protected by spin-group symmetries, a spin-singlet Cooper pairing may occur for the corresponding momenta. For the spin-singlet case, in analogy to conventional antiferromagnets, the 2×2 Cooper-pair potential matrix (gap function or order parameter) $\hat{\mathbf{\Delta}}(\mathbf{k})$ satisfies $\Delta_{\uparrow\uparrow}(\mathbf{k}) = \Delta_{\downarrow\downarrow}(\mathbf{k}) = 0$, $\Delta_{\downarrow\uparrow}(\mathbf{k}) = -\Delta_{\uparrow\downarrow}(\mathbf{k})$, and $\Delta_{\uparrow\downarrow}(\mathbf{k}) = \Delta_{\uparrow\downarrow}(-\mathbf{k})$ [151]. The matrix is unitary, with corresponding zero net spin average of the pairing state, and it describes even-parity wave Copper pairing, including the anisotropic, e.g., d-wave, pairing.

However, the altermagnetic spin-group symmetries also allow for spin-split and broken $\mathcal{T}$-symmetry parts of the Brillouin zone, where $\epsilon(s, \mathbf{k}) \neq \epsilon(-s, -\mathbf{k})$ and $A\mathbf{Hk} \neq \mathbf{k}$ (cf. fourth and sixth lines in Table II). These momenta can support spin-triplet Cooper pairing. In analogy to ferromagnets, the spin-triplet Cooper-pair potential matrix corresponding to a spin-split spin-up Fermi surface of the altermagnet, $\hat{\mathbf{\Delta}}^{(\uparrow)}(\mathbf{k})$, takes the form $\Delta^{(\uparrow)}_{\uparrow\downarrow}(\mathbf{k}) = \Delta^{(\uparrow)}_{\downarrow\uparrow}(\mathbf{k}) = \Delta^{(\uparrow)}_{\downarrow\downarrow}(\mathbf{k}) = 0$ and $\Delta^{(\uparrow)}_{\uparrow\uparrow}(\mathbf{k}) = -\Delta^{(\uparrow)}_{\uparrow\uparrow}(-\mathbf{k})$ [151]. The matrix in this case is nonunitary and describes odd-parity wave Copper pairing [151]. Unlike ferromagnets, however, the altermagnetic spin-group symmetries impose the presence of a counterpart spin-down Fermi surface with a corresponding $\hat{\mathbf{\Delta}}^{(\downarrow)}(\mathbf{k}')$ that satisfies $\Delta^{(\downarrow)}_{\uparrow\downarrow}(\mathbf{k}') = \Delta^{(\downarrow)}_{\downarrow\uparrow}(\mathbf{k}') = \Delta^{(\downarrow)}_{\uparrow\uparrow}(\mathbf{k}') = 0$, $\Delta^{(\downarrow)}_{\downarrow\downarrow}(\mathbf{k}') = -\Delta^{(\downarrow)}_{\downarrow\downarrow}(-\mathbf{k}')$, and $\Delta^{(\downarrow)}_{\downarrow\downarrow}(\mathbf{k}') = \Delta^{(\uparrow)}_{\uparrow\uparrow}(\mathbf{k})$, where $\mathbf{k}' = A\mathbf{Hk}$. On one hand, altermagnets can thus share the spin-triplet symmetry of Cooper pairing with ferromagnets. On the other hand, unlike ferromagnets, the altermagnetic spin-group symmetries protect a zero net spin average of the spin-triplet superconducting state. In the context of unconventional superconductivity, we again see that altermagnets can share features typical of ferromagnets or typical of antiferromagnets, and they can also show

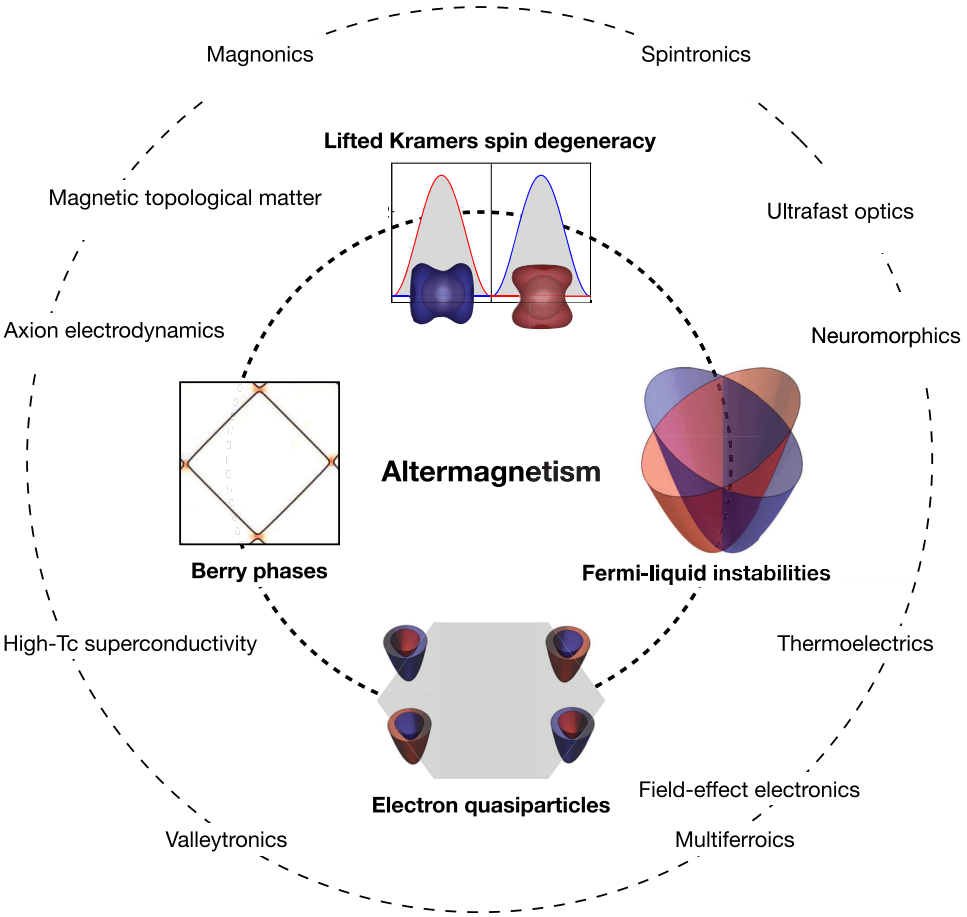

FIG. 14. Summary of the emerging research landscape of altermagnetism.

features unparalleled in either of the two conventional magnetic phases.

Apart from the compatibility of altermagnetism with the different types of Cooper pairing, altermagnetic fluctuations can provide mechanisms for generating electron pairing that have not been explored before. Since the electron-phonon coupling mechanism tends to be limited to the conventional spin-singlet *s*-wave pairing [151], altermagnets can be particularly relevant for the research of unconventional superconductivity, including both the spin-singlet and spin-triplet anisotropic types of Cooper pairing.

Finally, we foresee intriguing new physics at altermagnet or superconductor interfaces in areas including Andreev reflection [152] or Majorana fermion quasiparticles [153]. On one hand, the behavior of altermagnets at these interfaces can be reminiscent of conventional antiferromagnets when dominated by the spin-symmetry-protected nodal surface. On the other hand, interface orientations exposing the strong altermagnetic spin splitting can generate a phenomenology similar to the ferromagnet or superconductor interfaces. As in the case of bulk crystals, the research of interface effects can exploit the predicted broad range of altermagnetic material types.

V. CONCLUSION

In this work, we have described a third basic magnetic phase that emerges already on the fundamental level of nonrelativistic, uncorrelated band theory of nonfrustrated collinear magnets. The altermagnetic phase has unconventional spin-polarization orders in the direct physical space and reciprocal momentum space; this phase is systematically classified and described by symmetry-group theory, and it is predicted to be abundant among diverse material types. The significance of this unconventional *d*-wave (or higher even-parity wave) magnetic phase is further underlined by the unique ways in which altermagnetism can contribute to the development of fundamental physical concepts and to the research in modern condensed-matter physics fields. Given the still relatively early stage of our understanding of altermagnetism, and the limited space, our choice of discussion topics in this work should be regarded as broadly illustrative and provisional. We can anticipate that in the near future, altermagnetism will have an impact on other fields including magnetic topological matter or axion electrodynamics. Our current view of the emerging research landscape of altermagnetism is summarized in Fig. 14.

ACKNOWLEDGMENTS

We acknowledge fruitful interactions with Igor Mazin. This work was supported by Ministry of Education of the Czech Republic Grants No. LNSM-LNSpin and No. LM2018140, Czech Science Foundation Grant No. 19-28375X, EU FET Open RIA Grant No. 766566, SPIN + X (DFG SFB TRR 173 268565370), and Elasto-Q-Mat (DFG SFB TRR 288 422213477). We acknowledge the computing time granted on the supercomputer Mogon at Johannes Gutenberg University Mainz.

[1] Louis Néel, *Magnetism and Local Molecular Field*, Science **174**, 985 (1971).

[2] Libor Šmejkal, Allan H. MacDonald, Jairo Sinova, Satoru Nakatsuji, and Tomas Jungwirth, *Anomalous Hall Antiferromagnets*, Nat. Rev. Mater. **7**, 482 (2022).

[3] Libor Šmejkal, Rafael González-Hernández, Tomáš Jungwirth, and Jairo Sinova, *Crystal Time-Reversal Symmetry Breaking and Spontaneous Hall Effect in Collinear Antiferromagnets*, Sci. Adv. **6**, eaaz8809 (2020).

[4] Makoto Naka, Satoru Hayami, Hiroaki Kusunose, Yuki Yanagi, Yukitoshi Motome, and Hitoshi Seo, *Spin Current Generation in Organic Antiferromagnets*, Nat. Commun. **10**, 4305 (2019).

[5] Zexin Feng, Xiaorong Zhou, Libor Šmejkal, Lei Wu, Zengwei Zhu, Huixin Guo, Rafael González-Hernández, Xiaoning Wang, Han Yan, Peixin Qin, Xin Zhang, Haojiang Wu, Hongyu Chen, Ziang Meng, Li Liu, Zhengcai Xia, Jairo Sinova, Tomáš Jungwirth, and Zhiqi Liu, *An Anomalous Hall Effect in Altermagnetic Ruthenium Dioxide*, Nat. Electron. **5**, 735 (2022).

[6] Helena Reichlova, Rafael Lopes Seeger, Rafael González-Hernández, Ismaila Kounta, Richard Schlitz, Dominik Kriegner, Philipp Ritzinger, Michaela Lammel, Miina Leiviskä, Vaclav Petiček, Petr Doležal, Eva Schmoranzerova, Antonín Badura, Andy Thomas, Vincent Baltz, Lisa Michez, Jairo Sinova, Sebastian T. B. Goennenwein, Tomáš Jungwirth, and Libo Smejkal, *Macroscopic Time Reversal Symmetry Breaking Arising from Antiferromagnetic Zeeman Effect*, arXiv:2012.15651v1.

[7] I. I. Mazin, K. Koepernik, M. D. Johannes, Rafael González-Hernández, and Libor Šmejkal, *Prediction of Unconventional Magnetism in Doped* $FeSb_2$, Proc. Natl. Acad. Sci. U.S.A. **118**, e2108924118 (2021).

[8] Rafael González-Hernández, Libor Šmejkal, Karel Výborný, Yuta Yahagi, Jairo Sinova, Tomáš Jungwirth, and Jakub Železný, *Efficient Electrical Spin Splitter Based on Nonrelativistic Collinear Antiferromagnetism*, Phys. Rev. Lett. **126**, 127701 (2021).

[9] Makoto Naka, Yukitoshi Motome, and Hitoshi Seo, *Perovskite as a Spin Current Generator*, Phys. Rev. B **103**, 125114 (2021).

[10] Arnab Bose, Nathaniel J. Schreiber, Rakshit Jain, Ding-fu Shao, Hari P. Nair, Jiaxin Sun, Xiyue S. Zhang, David A. Muller, Evgeny Y. Tsymbal, Darrell G. Schlom, and Daniel C. Ralph, *Tilted Spin Current Generated by an Antiferromagnet*, Nat. Electron. **5**, 263 (2022).

[11] Hua Bai, Lei Han, X. Y. Feng, Y. J. Zhou, R. X. Su, Qian Wang, L. Y. Liao, W. X. Zhu, X. Z. Chen, Feng Pan, X. L. Fan, and Cheng Song, *Observation of Spin Splitting Torque in a Collinear Antiferromagnet* RuO_2, Phys. Rev. Lett. **128**, 197202 (2022).

[12] Shutaro Karube, Takahiro Tanaka, Daichi Sugawara, Naohiro Kadoguchi, Makoto Kohda, and Junsaku Nitta, *Observation of Spin-Splitter Torque in Collinear Antiferromagnetic* RuO_2, Phys. Rev. Lett. **129**, 137201 (2022).

[13] Libor Šmejkal, Anna Birk Hellenes, Rafael González-Hernández, Jairo Sinova, and Tomas Jungwirth, *Giant and Tunneling Magnetoresistance in Unconventional Collinear Antiferromagnets with Nonrelativistic Spin-Momentum Coupling*, Phys. Rev. X **12**, 011028 (2022).

[14] Ding-Fu Shao, Shu-Hui Zhang, Ming Li, Chang-Beom Eom, and Evgeny Y. Tsymbal, *Spin-Neutral Currents for Spintronics*, Nat. Commun. **12**, 7061 (2021).

[15] Hai-Yang Ma, Mengli Hu, Nana Li, Jianpeng Liu, Wang Yao, Jin-Feng Jia, and Junwei Liu, *Multifunctional Antiferromagnetic Materials with Giant Piezomagnetism and Noncollinear Spin Current*, Nat. Commun. **12**, 2846 (2021).

[16] Libor Šmejkal, Jairo Sinova, and Tomas Jungwirth, *Beyond Conventional Ferromagnetism and Antiferromagnetism: A Phase with Nonrelativistic Spin and Crystal Rotation Symmetry*, Phys. Rev. X **12**, 031042 (2022).

[17] Yusuke Noda, Kaoru Ohno, and Shinichiro Nakamura, *Momentum-Dependent Band Spin Splitting in Semiconducting* MnO_2*: A Density Functional Calculation*, Phys. Chem. Chem. Phys. **18**, 13294 (2016).

[18] Kyo-Hoon Ahn, Atsushi Hariki, Kwan-Woo Lee, and Jan Kuneš, *Antiferromagnetism in* RuO_2 *as d-wave Pomeranchuk Instability*, Phys. Rev. B **99**, 184432 (2019).

[19] Satoru Hayami, Yuki Yanagi, and Hiroaki Kusunose, *Momentum-Dependent Spin Splitting by Collinear Antiferromagnetic Ordering*, J. Phys. Soc. Jpn. **88**, 123702 (2019).

[20] Lin-Ding Yuan, Zhi Wang, Jun-Wei Luo, Emmanuel I. Rashba, and Alex Zunger, *Giant Momentum-Dependent Spin Splitting in Centrosymmetric Low-Z Antiferromagnets*, Phys. Rev. B **102**, 014422 (2020).

[21] Satoru Hayami, Yuki Yanagi, and Hiroaki Kusunose, *Bottom-up Design of Spin-Split and Reshaped Electronic Band Structures in Antiferromagnets without Spin-Orbit Coupling: Procedure on the Basis of Augmented Multipoles*, Phys. Rev. B **102**, 144441 (2020).

[22] Lin-Ding Yuan, Zhi Wang, Jun-Wei Luo, and Alex Zunger, *Prediction of Low-Z Collinear and Noncollinear Antiferromagnetic Compounds Having Momentum-Dependent Spin Splitting Even without Spin-Orbit Coupling*, Phys. Rev. Mater. **5**, 014409 (2021).

[23] Sergei A. Egorov and Robert A. Evarestov, *Colossal Spin Splitting in the Monolayer of the Collinear Antiferromagnet* MnF_2, J. Phys. Chem. Lett. **12**, 2363 (2021).

[24] Pengfei Liu, Jiayu Li, Jingzhi Han, Xiangang Wan, and Qihang Liu, *Spin-Group Symmetry in Magnetic Materials with Negligible Spin-Orbit Coupling*, Phys. Rev. X **12**, 021016 (2022).

[25] Jian Yang, Zheng-Xin Liu, and Chen Fang, *Symmetry Invariants of Spin Space Groups in Magnetic Materials*, arXiv:2105.12738.

[26] W. F. Brinkman and R. J. Elliott, *Theory of Spin-Space Groups*, Proc. R. Soc. A **294**, 343 (1966).

[27] D. B. Litvin and W. Opechowski, *Spin Groups*, Physica **76**, 538 (1974).

[28] D. B. Litvin, *Spin Point Groups*, Acta Crystallogr. Sect. A **33**, 279 (1977).

[29] A. Schofield, *There and Back Again: From Magnets to Superconductors*, Physics **2**, 93 (2009).

[30] Qimiao Si, Rong Yu, and Elihu Abrahams, *High-Temperature Superconductivity in Iron Pnictides and Chalcogenides*, Nat. Rev. Mater. **1**, 16017 (2016).

[31] Congjun Wu, Kai Sun, Eduardo Fradkin, and Shou-Cheng Zhang, *Fermi Liquid Instabilities in the Spin Channel*, Phys. Rev. B **75**, 115103 (2007).

[32] Laura Classen, Andrey V. Chubukov, Carsten Honerkamp, and Michael M. Scherer, *Competing Orders at Higher-Order Van Hove Points*, Phys. Rev. B **102**, 125141 (2020).

[33] R. A. Borzi, S. A. Grigera, J. Farrell, R. S. Perry, S. J. S. Lister, S. L. Lee, D. A. Tennant, Y. Maeno, and A. P. Mackenzie, *Formation of a Nematic Fluid at High Fields in* $Sr_3Ru_2O_7$, Science **315**, 214 (2007).

[34] F. Duncan M. Haldane, *Nobel Lecture: Topological Quantum Matter*, Rev. Mod. Phys. **89**, 040502 (2017).

[35] J. Georg Bednorz and K. Alex Müller, *Perovskite-Type Oxides—The New Approach to High-*T_c *Superconductivity. Nobel Lecture*, Angew. Chem., Int. Ed. Engl. **27**, 735 (1988).

[36] Horst L. Stormer, *Nobel Lecture: The Fractional Quantum Hall Effect*, Rev. Mod. Phys. **71**, 875 (1999).

[37] Naoto Nagaosa, Jairo Sinova, Shigeki Onoda, A. H. MacDonald, and N. P. Ong, *Anomalous Hall Effect*, Rev. Mod. Phys. **82**, 1539 (2010).

[38] Jairo Sinova, Sergio O. Valenzuela, J. Wunderlich, C. H. Back, and T. Jungwirth, *Spin Hall Effects*, Rev. Mod. Phys. **87**, 1213 (2015).

[39] T. Jungwirth, X. Marti, P. Wadley, and J. Wunderlich, *Antiferromagnetic Spintronics*, Nat. Nanotechnol. **11**, 231 (2016).

[40] A. Manchon, J. Železný, I. M. Miron, T. Jungwirth, J. Sinova, A. Thiaville, K. Garello, and P. Gambardella, *Current-Induced Spin-Orbit Torques in Ferromagnetic and Antiferromagnetic Systems*, Rev. Mod. Phys. **91**, 035004 (2019).

[41] *Contemporary Concepts of Condensed Matter Science*, edited by M. Franz and L. Molenkamp, Topological Insulators Vol. 6 (Elsevier, New York, 2013).

[42] Yoshinori Tokura, Kenji Yasuda, and Atsushi Tsukazaki, *Magnetic Topological Insulators*, Nat. Rev. Phys. **1**, 126 (2019).

[43] Satoru Nakatsuji and Ryotaro Arita, *Topological Magnets: Functions Based on Berry Phase and Multipoles*, Annu. Rev. Condens. Matter Phys. **13**, 119 (2022).

[44] Kartik Samanta, Marjana Ležaić, Maximilian Merte, Frank Freimuth, Stefan Blügel, and Yuriy Mokrousov, *Crystal Hall and Crystal Magneto-Optical Effect in Thin Films of* $SrRuO_3$, J. Appl. Phys. **127**, 213904 (2020).

[45] Makoto Naka, Satoru Hayami, Hiroaki Kusunose, Yuki Yanagi, Yukitoshi Motome, and Hitoshi Seo, *Anomalous Hall Effect in κ-Type Organic Antiferromagnets*, Phys. Rev. B **102**, 075112 (2020).

[46] Makoto Naka, Yukitoshi Motome, and Hitoshi Seo, *Anomalous Hall Effect in Antiferromagnetic Perovskites*, arXiv:2208.11823.

[47] S. López-Moreno, A. H. Romero, J. Mejía-López, A. Muñoz, and Igor V. Roshchin, *First-Principles Study of Electronic, Vibrational, Elastic, and Magnetic Properties of* FeF_2 *as a Function of Pressure*, Phys. Rev. B **85**, 134110 (2012).

[48] S. López-Moreno, A. H. Romero, J. Mejía-López, and A. Muñoz, *First-Principles Study of Pressure-Induced Structural Phase Transitions in* MnF_2, Phys. Chem. Chem. Phys. **18**, 33250 (2016).

[49] Louis Néel, *Some New Results on Antiferromagnetism and Ferromagnetism*, Rev. Mod. Phys. **25**, 58 (1953).

[50] N. Kurti, *Selected Works of Louis Neel*, 1st ed. (CRC Press, London, 1988).

[51] T. Berlijn, P. C. Snijders, O. Delaire, H. D. Zhou, T. A. Maier, H. B. Cao, S. X. Chi, M. Matsuda, Y. Wang, M. R. Koehler, P. R. C. Kent, and H. H. Weitering, *Itinerant Antiferromagnetism in* RuO_2, Phys. Rev. Lett. **118**, 077201 (2017).

[52] Z. H. Zhu, J. Strempfer, R. R. Rao, C. A. Occhialini, J. Pelliciari, Y. Choi, T. Kawaguchi, H. You, J. F. Mitchell, Y. Shao-Horn, and R. Comin, *Anomalous Antiferromagnetism in Metallic* RuO_2 *Determined by Resonant X-ray Scattering*, Phys. Rev. Lett. **122**, 017202 (2019).

[53] S. W. Lovesey, D. D. Khalyavin, and G. van der Laan, *Magnetic Properties of Ruthenium Dioxide (*RuO_2*) and Charge-Magnetic Interference in Bragg Diffraction of Circularly Polarized X-rays*, Phys. Rev. B **105**, 014403 (2022).

[54] Connor A. Occhialini, Valentina Bisogni, Hoydoo You, Andi Barbour, Ignace Jarrige, J. F. Mitchell, Riccardo Comin, and Jonathan Pelliciari, *Local Electronic Structure of Rutile* RuO_2, Phys. Rev. Res. **3**, 033214 (2021).

[55] K. Ishizaka *et al.*, *Giant Rashba-Type Spin Splitting in Bulk BiTeI*, Nat. Mater. **10**, 521 (2011).

[56] Aleksandr F. Andreev and V. I. Marchenko, *Symmetry and the Macroscopic Dynamics of Magnetic Materials*, Usp. Fiz. Nauk **130**, 39 (1980).

[57] Peng-Jie Guo, Yi-Wen Wei, Kai Liu, Zheng-Xin Liu, and Zhong-Yi Lu, *Eightfold Degenerate Fermions in Two Dimensions*, Phys. Rev. Lett. **127**, 176401 (2021).

[58] Pengfei Liu, Jingzhi Han, and Qihang Liu, *Flavor Weyl Fermions Protected by SU(2) Isospin Symmetry in Spin-Orbit-Free Antiferromagnetic Semimetals*, arXiv:2107.09984.

[59] A. Corticelli, R. Moessner, and P. A. McClarty, *Spin-Space Groups and Magnon Band Topology*, Phys. Rev. B **105**, 064430 (2022).

[60] Ilja Turek, *Altermagnetism and Magnetic Groups with Pseudoscalar Electron Spin*, Phys. Rev. B **106**, 094432 (2022).

[61] Patrick M. Lenggenhager, Xiaoxiong Liu, Titus Neupert, and Tomáš Bzdušek, *Triple Nodal Points Characterized by Their Nodal-Line Structure in All Magnetic Space Groups*, Phys. Rev. B **106**, 085128 (2022).

[62] L. D. Landau and E. M. Lifshitz, in *Electrodynamics of Continuous Media*, Course of Theoretical Physics Vol. 8, 2nd ed. (Pergamon Press, Oxford, 1965).

[63] N. V. Shubnikov and A. V. Belov, *Colored Symmetry* (MacMillan Publishers, New York, 1964).

[64] B. A. Tavger and V. M. Zaitsev, *Magnetic Symmetry of Crystals*, Sov. Phys. JETP **3**, 430 (1956).

[65] C. J. Bradley and A. P. Cracknell, *The Mathematical Theory of Symmetry in Solids* (Oxford University Press, New York, 1972).

[66] D. B. Litvin, *Magnetic Group Tables* (International Union of Crystallography, Chester, England, 2013).

[67] Samuel V. Gallego, J. Manuel Perez-Mato, Luis Elcoro, Emre S. Tasci, Robert M. Hanson, Koichi Momma, Mois I. Aroyo, and Gotzon Madariaga, *MAGNDATA: Towards a Database of Magnetic Structures. I. The Commensurate Case*, J. Appl. Crystallogr. **49**, 1750 (2016).

[68] A. Corticelli, R Moessner, and P. A. McClarty, *Spin-Space Groups and Magnon Band Topology*, Phys. Rev. B **105**, 064430 (2022).

[69] E. A. Turov, *Physical Properties of Magnetically Ordered Crystals* (Academic Press, New York, 1965).

[70] A. S. Núñez, R. A. Duine, Paul Haney, and A. H. MacDonald, *Theory of Spin Torques and Giant Magnetoresistance in Antiferromagnetic Metals*, Phys. Rev. B **73**, 214426 (2006).

[71] Christoph Sürgers, Gerda Fischer, Patrick Winkel, and Hilbert V. Löhneysen, *Large Topological Hall Effect in the Non-collinear Phase of an Antiferromagnet*, Nat. Commun. **5**, 3400 (2014).

[72] Christoph Sürgers, Wolfram Kittler, Thomas Wolf, and Hilbert V. Löhneysen, *Anomalous Hall Effect in the Non-collinear Antiferromagnet* Mn_5Si_3, AIP Adv. **6**, 055604 (2016).

[73] Nirmal J. Ghimire, A. S. Botana, J. S. Jiang, Junjie Zhang, Y.-S. Chen, and J. F. Mitchell, *Large Anomalous Hall Effect in the Chiral-Lattice Antiferromagnet* $CoNb_3S_6$, Nat. Commun. **9**, 3280 (2018).

[74] Joel E. Moore, *The Birth of Topological Insulators*, Nature (London) **464**, 194 (2010).

[75] Xin Chen, Duo Wang, Linyang Li, and Biplab Sanyal, *Room Temperature Two-Dimensional Antiferromagnetic Weyl Semimetal CrO with Giant Spin-Splitting and Spin-Momentum Locked Transport*, arXiv:2104.07390.

[76] Takuya Okugawa, Kaoru Ohno, Yusuke Noda, and Shinichiro Nakamura, *Weakly Spin-Dependent Band Structures of Antiferromagnetic Perovskite* $LaMO_3$ *(*M = Cr*, Mn, Fe)*, J. Phys. Condens. Matter **30**, 075502 (2018).

[77] H. A. Kramers, *Théorie Générale de la Rotation Paramagnétique Dans les Cristaux.*, Proc. Amsterdam Acad. **33** (1930).

[78] E. Wigner, *Ueber die Operation der Zeitumkehr in der Quantenmechanik, Nachrichten von der Gesellschaft der Wissenschaften zu Göttingen*, Mathematisch-Physikalische Klasse **1932**, 546 (1932).

[79] Barry Bradlyn, L. Elcoro, Jennifer Cano, M. G. Vergniory, Zhijun Wang, C. Felser, M. I. Aroyo, and B. Andrei Bernevig, *Topological Quantum Chemistry*, Nature (London) **547**, 298 (2017).

[80] Libor Šmejkal, Yuriy Mokrousov, Binghai Yan, and Allan H. MacDonald, *Topological Antiferromagnetic Spintronics*, Nat. Phys. **14**, 242 (2018).

[81] *Topology in Magnetism*, edited by Jiadong Zang, Vincent Cros, and Axel Hoffmann, Springer Series in Solid-State Sciences Vol. 192 (Springer International Publishing, Cham, 2018).

[82] M. G. Vergniory, L. Elcoro, Claudia Felser, Nicolas Regnault, B. Andrei Bernevig, and Zhijun Wang, *A Complete Catalogue of High-Quality Topological Materials*, Nature (London) **566**, 480 (2019).

[83] Yuanfeng Xu, Luis Elcoro, Zhi Da Song, Benjamin J. Wieder, M. G. Vergniory, Nicolas Regnault, Yulin Chen, Claudia Felser, and B. Andrei Bernevig, *High-Throughput Calculations of Magnetic Topological Materials*, Nature (London) **586**, 702 (2020).

[84] Luis Elcoro, Benjamin J. Wieder, Zhida Song, Yuanfeng Xu, Barry Bradlyn, and B. Andrei Bernevig, *Magnetic Topological Quantum Chemistry*, Nat. Commun. **12**, 5965 (2021).

[85] Claude Chappert, Albert Fert, and Frédéric Nguyen Van Dau, *The Emergence of Spin Electronics in Data Storage*, Nat. Mater. **6**, 813 (2007).

[86] D. C. Ralph and M. D. Stiles, *Spin Transfer Torques*, J. Magn. Magn. Mater. **320**, 1190 (2008).

[87] Sabpreet Bhatti, Rachid Sbiaa, Atsufumi Hirohata, Hideo Ohno, Shunsuke Fukami, and S. N. Piramanayagam, *Spintronics Based Random Access Memory: A Review*, Mater. Today **20**, 530 (2017).

[88] Roland Winkler, *Spin–Orbit Coupling Effects in Two-Dimensional Electron and Hole Systems*, Springer Tracts in Modern Physics (Springer, Berlin, Heidelberg, 2003), Vol. 191.

[89] N. P. Armitage, E. J. Mele, and Ashvin Vishwanath, *Weyl and Dirac Semimetals in Three-Dimensional Solids*, Rev. Mod. Phys. **90**, 015001 (2018).

[90] X. Marti, I. Fina, C. Frontera, Jian Liu, P. Wadley, Q. He, R. J. Paull, J. D. Clarkson, J. Kudrnovský, I. Turek, J. Kuneš, D. Yi, J.-H. Chu, C. T. Nelson, L. You, E. Arenholz, S. Salahuddin, J. Fontcuberta, T. Jungwirth, and R. Ramesh, *Room-Temperature Antiferromagnetic Memory Resistor*, Nat. Mater. **13**, 367 (2014).

[91] M. M. Otrokov *et al.*, *Prediction and Observation of an Antiferromagnetic Topological Insulator*, Nature (London) **576**, 416 (2019).

[92] J. Železný, H. Gao, K. Výborný, J. Zemen, J. Mašek, Aurélien Manchon, J. Wunderlich, Jairo Sinova, and T. Jungwirth, *Relativistic Néel-Order Fields Induced by Electrical Current in Antiferromagnets*, Phys. Rev. Lett. **113**, 157201 (2014).

[93] P. Wadley *et al.*, *Electrical Switching of an Antiferromagnet*, Science **351**, 587 (2016).

[94] Libor Šmejkal, J. Železný, J. Sinova, and T. Jungwirth, *Electric Control of Dirac Quasiparticles by Spin-Orbit Torque in an Antiferromagnet*, Phys. Rev. Lett. **118**, 106402 (2017).

[95] H. J. Elmers, S. V. Chernov, S. W. D'Souza, S. P. Bommanaboyena, S. Yu Bodnar, K. Medjanik, S. Babenkov, O. Fedchenko, D. Vasilyev, S. Y. Agustsson, C. Schlueter, A. Gloskovskii, Yu Matveyev, V. N. Strocov,

Y. Skourski, L. Šmejkal, J. Sinova, J. Minár, M. Kläui, G. Schönhense, and M. Jourdan, *Néel Vector Induced Manipulation of Valence States in the Collinear Antiferromagnet* Mn_2Au, ACS Nano **14**, 17554 (2020).

[96] Olena Fedchenko, Libor Smejkal, Michael Kallmayer, Yarina Lytvynenko, Katerina Medjanik, Sergey Babenkov, Dmitry Vasilyev, Matthias Klaeui, Jure Demsar, Gerd Schoenhense, Martin Jourdan, Jairo Sinova, and Hans-Joachim Elmers, *Direct Observation of Antiferromagnetic Parity Violation in the Electronic Structure of* Mn_2Au, arXiv:2110.12186.

[97] Revaz Ramazashvili, *Kramers Degeneracy in a Magnetic Field and Zeeman Spin-Orbit Coupling in Antiferromagnetic Conductors*, Phys. Rev. Lett. **101**, 137202 (2008).

[98] Revaz Ramazashvili, *Kramers Degeneracy in a Magnetic Field and Zeeman Spin-Orbit Coupling in Antiferromagnetic Conductors*, Phys. Rev. B **79**, 184432 (2009).

[99] Emil J. Rozbicki, James F. Annett, Jean-René Souquet, and Andrew P. Mackenzie, *Spin-Orbit Coupling and k-Dependent Zeeman Splitting in Strontium Ruthenate*, J. Phys. Condens. Matter **23**, 094201 (2011).

[100] T. Suzuki, R. Chisnell, A. Devarakonda, Y. T. Liu, W. Feng, D. Xiao, J. W. Lynn, and J. G. Checkelsky, *Large Anomalous Hall Effect in a Half-Heusler Antiferromagnet*, Nat. Phys. **12**, 1119 (2016).

[101] Kunihiko Yamauchi, Paolo Barone, and Silvia Picozzi, *Bulk Rashba Effect in Multiferroics: A Theoretical Prediction for* $BiCoO_3$, Phys. Rev. B **100**, 245115 (2019).

[102] Benjamin Schrunk, Yevhen Kushnirenko, Brinda Kuthanazhi, Junyeong Ahn, Lin-Lin Wang, Evan O'Leary, Kyungchan Lee, Andrew Eaton, Alexander Fedorov, Rui Lou, Vladimir Voroshnin, Oliver J. Clark, Jaime Sánchez-Barriga, Sergey L. Bud'ko, Robert-Jan Slager, Paul C. Canfield, and Adam Kaminski, *Emergence of Fermi Arcs Due to Magnetic Splitting in an Antiferromagnet*, Nature (London) **603**, 610 (2022).

[103] I. I. Pomeranchuk, *On the Stability of a Fermi Liquid*, Phys. JETP **8**, 361 (1959).

[104] Sergei A. Egorov, Daniel B. Litvin, and Robert A. Evarestov, *Antiferromagnetism-Induced Spin Splitting in Systems Described by Magnetic Layer Groups*, J. Phys. Chem. C **125**, 16147 (2021).

[105] John R. Schaibley, Hongyi Yu, Genevieve Clark, Pasqual Rivera, Jason S. Ross, Kyle L. Seyler, Wang Yao, and Xiaodong Xu, *Valleytronics in 2D Materials*, Nat. Rev. Mater. **1**, 16055 (2016).

[106] A. Marmodoro, L. Šmejkal, J. Sinova, and T. Jungwirth (to be published).

[107] S. V. Halilov, H. Eschrig, A. Y. Perlov, and P. M. Oppeneer, *Adiabatic Spin Dynamics from Spin-Density-Functional Theory: Application to Fe, Co, and Ni*, Phys. Rev. B **58**, 293 (1998).

[108] Alberto Marmodoro, Sergiy Mankovsky, Hubert Ebert, Jan Minár, and Ondej Ondej Ondejšipr, *Electric Field Control of Magnons in Magnetic Thin Films: Ab Initio Predictions for 2D Metallic Heterostructures*, Phys. Rev. B **105**, 174411 (2022).

[109] Sergio M. Rezende, Antonio Azevedo, and Roberto L. Rodríguez-Suárez, *Introduction to Antiferromagnetic Magnons*, J. Appl. Phys. **126**, 151101 (2019).

[110] R. Lebrun, A. Ross, S. A. Bender, A. Qaiumzadeh, L. Baldrati, J. Cramer, A. Brataas, R. A. Duine, and M. Kläui, *Tunable Long-Distance Spin Transport in a Crystalline Antiferromagnetic Iron Oxide*, Nature (London) **561**, 222 (2018).

[111] M. V. Berry, *Quantal Phase Factors Accompanying Adiabatic Changes*, Proc. R. Soc. A **392**, 45 (1984).

[112] Dimitrie Culcer, Allan MacDonald, and Qian Niu, *Anomalous Hall Effect in Paramagnetic Two-Dimensional Systems*, Phys. Rev. B **68**, 045327 (2003).

[113] Tamara S. Nunner, N. A. Sinitsyn, Mario F. Borunda, V. K. Dugaev, A. A. Kovalev, Ar. Abanov, Carsten Timm, T. Jungwirth, Jun-ichiro Inoue, A. H. MacDonald, and Jairo Sinova, *Anomalous Hall Effect in a Two-Dimensional Electron Gas*, Phys. Rev. B **76**, 235312 (2007).

[114] V. K. Dugaev, J. Barnaś, M. Taillefumier, B. Canals, C. Lacroix, and P. Bruno, *Anomalous Hall Effect and Berry Phase in Two-Dimensional Magnetic Structures*, J. Phys. Conf. Ser. **104**, 012018 (2008).

[115] Di Xiao, Ming Che Chang, and Qian Niu, *Berry Phase Effects on Electronic Properties*, Rev. Mod. Phys. **82**, 1959 (2010).

[116] Hitoshi Seo and Makoto Naka, *Antiferromagnetic State in κ-type Molecular Conductors: Spin Splitting and Mott Gap*, J. Phys. Soc. Jpn. **90**, 064713 (2021).

[117] Ding Fu Shao, Jun Ding, Gautam Gurung, Shu Hui Zhang, and Evgeny Y. Tsymbal, *Interfacial Crystal Hall Effect Reversible by Ferroelectric Polarization*, Phys. Rev. Appl. **15**, 024057 (2021).

[118] M. Z. Hasan and C. L. Kane, *Colloquium: Topological Insulators*, Rev. Mod. Phys. **82**, 3045 (2010).

[119] K. V. Klitzing, G. Dorda, and M. Pepper, *New Method for High-Accuracy Determination of the Fine-Structure Constant Based on Quantized Hall Resistance*, Phys. Rev. Lett. **45**, 494 (1980).

[120] K. S. Novoselov, Z. Jiang, Y. Zhang, S. V. Morozov, H. L. Stormer, U. Zeitler, J. C. Maan, G. S. Boebinger, P. Kim, and A. K. Geim, *Room-Temperature Quantum Hall Effect in Graphene*, Science **315**, 1379 (2007).

[121] C.-Z. Chang *et al.*, *Experimental Observation of the Quantum Anomalous Hall Effect in a Magnetic Topological Insulator*, Science **340**, 167 (2013).

[122] Yujun Deng, Yijun Yu, Meng Zhu Shi, Zhongxun Guo, Zihan Xu, Jing Wang, Xian Hui Chen, and Yuanbo Zhang, *Quantum Anomalous Hall Effect in Intrinsic Magnetic Topological Insulator* $MnBi_2Te_4$, Science **367**, 895 (2020).

[123] Samuel D. Bader and S. S. P. Parkin, *Spintronics*, Annu. Rev. Condens. Matter Phys. **1**, 71 (2010).

[124] Peter Wadley, Sonka Reimers, Michal J. Grzybowski, Carl Andrews, Mu Wang, Jasbinder S. Chauhan, Bryan L. Gallagher, Richard P. Campion, Kevin W. Edmonds, Sarnjeet S. Dhesi, Francesco Maccherozzi, Vit Novak, Joerg Wunderlich, and Tomas Jungwirth, *Current Polarity-Dependent Manipulation of Antiferromagnetic Domains*, Nat. Nanotechnol. **13**, 362 (2018).

[125] Yang Zhang, Qiunan Xu, Klaus Koepernik, Roman Rezaev, Oleg Janson, Jakub Železný, Tomáš Jungwirth, Claudia Felser, Jeroen van den Brink, and Yan Sun, *Different Types of Spin Currents in the Comprehensive*

Materials Database of Nonmagnetic Spin Hall Effect, npj Comput. Mater. **7**, 167 (2021).

[126] Arne Brataas, Andrew D. Kent, and Hideo Ohno, *Current-Induced Torques in Magnetic Materials*, Nat. Mater. **11**, 372 (2012).

[127] R. A. Duine, Kyung-Jin Lee, Stuart S. P. Parkin, and M. D. Stiles, *Synthetic Antiferromagnetic Spintronics*, Nat. Phys. **14**, 217 (2018).

[128] S. Schlauderer, C. Lange, S. Baierl, T. Ebnet, C. P. Schmid, D. C. Valovcin, A. K. Zvezdin, A. V. Kimel, R. V. Mikhaylovskiy, and R. Huber, *Temporal and Spectral Fingerprints of Ultrafast All-Coherent Spin Switching*, Nature (London) **569**, 383 (2019).

[129] R. Landauer, *Irreversibility and Heat Generation in the Computing Process*, IBM J. Res. Dev. **5**, 183 (1961).

[130] Charles H. Bennett, *The Thermodynamics of Computation —A Review*, Int. J. Theor. Phys. **21**, 905 (1982).

[131] Jeongmin Hong, Brian Lambson, Scott Dhuey, and Jeffrey Bokor, *Experimental Test of Landauer's Principle in Single-Bit Operations on Nanomagnetic Memory Bits*, Sci. Adv. **2** (2016).

[132] R. Gaudenzi, E. Burzurí, S. Maegawa, H. S. J. van der Zant, and F. Luis, *Quantum Landauer Erasure with a Molecular Nanomagnet*, Nat. Phys. **14**, 565 (2018).

[133] A. V. Kimel, A. M. Kalashnikova, A. Pogrebna, and A. K. Zvezdin, *Fundamentals and Perspectives of Ultrafast Photoferroic Recording*, Phys. Rep. **852**, 1 (2020).

[134] Z. Kašpar, M. Surýnek, J. Zubáč, F. Krizek, V. Novák, R. P. Campion, M. S. Wörnle, P. Gambardella, X. Marti, P. Němec, K. W. Edmonds, S. Reimers, O. J. Amin, F. Maccherozzi, S. S. Dhesi, P. Wadley, J. Wunderlich, K. Olejník, and T. Jungwirth, *Quenching of an Antiferromagnet into High Resistivity States Using Electrical or Ultrashort Optical Pulses*, National electronics review **4**, 30 (2021).

[135] Jan Zubáč, Zdeněk Kašpar, Filip Krizek, Tobias Förster, Richard P. Campion, Vít Novák, Tomáš Jungwirth, and Kamil Olejník, *Hysteretic Effects and Magnetotransport of Electrically Switched CuMnAs*, Phys. Rev. B **104**, 184424 (2021).

[136] Filip Krizek, Sonka Reimers, Zdeněk Kašpar, Alberto Marmodoro, Jan Michalička, Ondej Man, Alexander Edstrom, Oliver J. Amin, Kevin W. Edmonds, Richard P. Campion, Francesco Maccherozzi, Sarnjeet S. Dnes, Jan Zubáč, Jakub Železný, Karel Výborný, Kamil Olejník, Vít Novák, Jan Rusz, Juan C. Idrobo, Peter Wadley, and Tomas Jungwirth, *Atomically Sharp Domain Walls in an Antiferromagnet*, Sci. Adv. **8**, eabn3535 (2022).

[137] Alexey V. Kimel and Mo Li, *Writing Magnetic Memory with Ultrashort Light Pulses*, Nat. Rev. Mater. **4**, 189 (2019).

[138] Gerrit E. W. Bauer, Eiji Saitoh, and Bart J. Van Wees, *Spin Caloritronics*, Nat. Mater. **11**, 391 (2012).

[139] Masaki Mizuguchi and Satoru Nakatsuji, *Energy-Harvesting Materials Based on the Anomalous Nernst Effect*, Sci. Technol. Adv. Mater. **20**, 262 (2019).

[140] Qing Jie, Rongwei Hu, Emil Bozin, A. Llobet, I. Zaliznyak, C. Petrovic, and Q. Li, *Electronic Thermoelectric Power Factor and Metal-Insulator Transition in* $FeSb_2$, Phys. Rev. B **86**, 115121 (2012).

[141] S. Meyer, Y. T. Chen, S. Wimmer, M. Althammer, T. Wimmer, R. Schlitz, S. Geprags, H. Huebl, D. Kodderitzsch, H. Ebert, G. E. W. Bauer, R. Gross, and S. T. B. Goennenwein, *Observation of the Spin Nernst Effect*, Nat. Mater. **16**, 977 (2017).

[142] Hantao Zhang and Ran Cheng, *A Perspective on Magnon Spin Nernst Effect in Antiferromagnets*, Appl. Phys. Lett. **120**, 090502 (2022).

[143] Tomasz Dietl and Hideo Ohno, *Dilute Ferromagnetic Semiconductors: Physics and Spintronic Structures*, Rev. Mod. Phys. **86**, 187 (2014).

[144] T. Jungwirth, J. Wunderlich, V. Novák, K. Olejník, B. L. Gallagher, R. P. Campion, K. W. Edmonds, A. W. Rushforth, A. J. Ferguson, and P. Němec, *Spin-Dependent Phenomena and Device Concepts Explored in (Ga,Mn)As*, Rev. Mod. Phys. **86**, 855 (2014).

[145] R. D. Gonzalez Betancourt, J. Zubáč, R. J. Gonzalez-Hernandez, K. Geishendorf, Z. Šobá, G. Springholz, K. Výborný, K. Olejník, L. Šmejkal, J. Sinova, T. Jungwirth, S. T. B. Goennenwein, A. Thomas, H. Reichlová, J. Železný, and D. Kriegner, *Spontaneous Anomalous Hall Effect Arising from Antiparallel Magnetic Order in a Semiconductor*, arXiv:2112.06805.

[146] Georgii A. Illarionov, Sofia M. Morozova, Vladimir V. Chrishtop, Mari-Ann Einarsrud, and Maxim I. Morozov, *Memristive* TiO_2*: Synthesis, Technologies, and Applications,* Front. Chem. **8**, 724 (2020).

[147] Writam Banerjee, Alireza Kashir, and Stanislav Kamba, *Hafnium Oxide* (HfO_2)*—A Multifunctional Oxide: A Review on the Prospect and Challenges of Hafnium Oxide in Resistive Switching and Ferroelectric Memories*, Small **18**, 2107575 (2022).

[148] R. Ramesh and Nicola A. Spaldin, *Multiferroics: Progress and Prospects in Thin Films*, Nat. Mater. **6**, 21 (2007).

[149] Satadeep Bhattacharjee, Eric Bousquet, and Philippe Ghosez, *Engineering Multiferroism in* $CaMnO_3$, Phys. Rev. Lett. **102**, 117602 (2009).

[150] Igor I. Mazin, *Notes on Altermagnetism and Superconductivity*, arXiv:2203.05000.

[151] Manfred Sigrist and Kazuo Ueda, *Phenomenological Theory of Unconventional Superconductivity*, Rev. Mod. Phys. **63**, 239 (1991).

[152] I. I. Mazin, A. A. Golubov, and B. Nadgorny, *Probing Spin Polarization with Andreev Reflection: A Theoretical Basis*, J. Appl. Phys. **89**, 7576 (2001).

[153] Karsten Flensberg, Felix von Oppen, and Ady Stern, *Engineered Platforms for Topological Superconductivity and Majorana Zero Modes*, Nat. Rev. Mater. **6**, 944 (2021).